CHALMERS

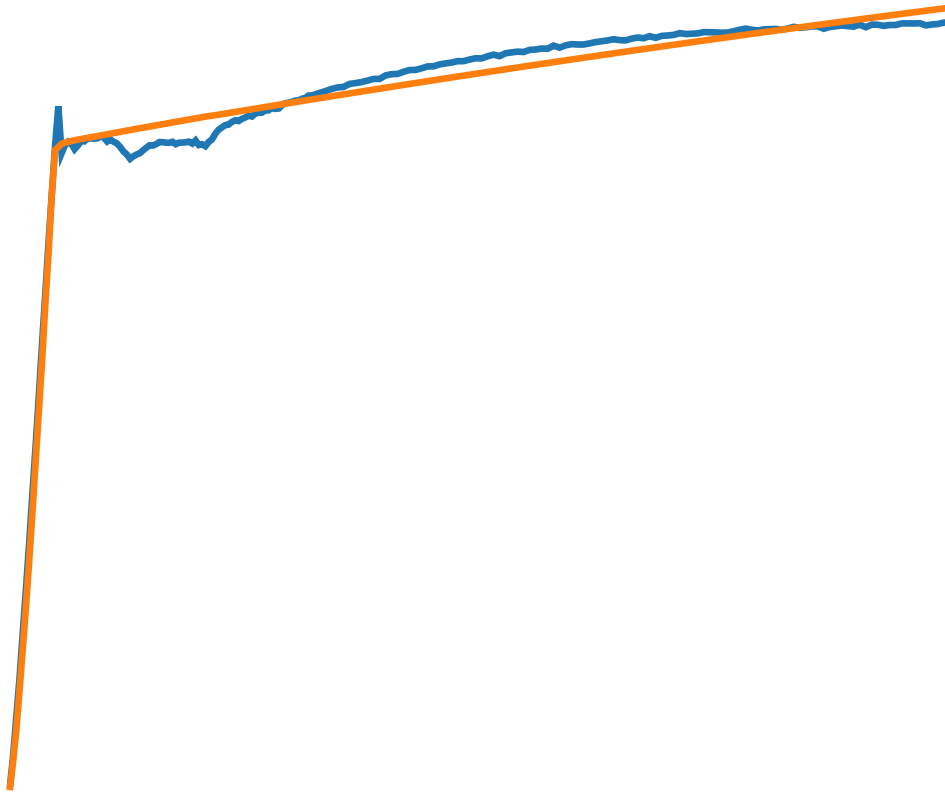## UNIVERSITY OF TECHNOLOGY

Finite Element Model Calibration with Digital Image Correlation

Master's thesis in Applied Mechanics

LOTTA BERGBOM

Finite Element Model Calibration with Digital Image Correlation

LOTTA BERGBOM

Finite Element Model Calibration with Digital Image Correlation
LOTTA BERGBOM

Cover: Force as a function of time obtained from experimental data and simulated data respectively.

Finite Element Model Calibration with Digital Image Correlation
LOTTA BERGBOM
Department of Industrial and Materials Science
Chalmers University of Technology

Abstract

Finite Element (FE) models are widely used to predict the mechanical behaviour of materials and components when subjected to different loads. In the industry, this is a valuable way to reduce the number of physical experiments and, thereby, costs when developing new products. With many actors trying to become more material efficient, new materials with sometimes complex structures are employed or the limits of how much the material is loaded are pushed. As a consequence of this, the need for adequate and accurate material models in the FE modelling increases.

Digital Image Correlation(DIC) is a non-contact measurement technique used to measure displacements and strains locally on a surface in space and time. The goal of this thesis is to use DIC data to calibrate some typical material models used in FE modelling. The value and potential of the proposed calibration method is evaluated. The work is performed in collaboration with Research Institutes of Sweden AB (RISE) who has extensive experience with physical experiments, modelling and DIC. As there already existed test results from tensile tests made of steel, these were used when developing the calibration method. For later applications more complicated material models are of interest but for concept testing, the choice of material model is less important and therefore the relatively simple linear isotropic elasticity and von Mises plasticity with linear hardening are chosen. The work was mainly divided into two parts. The first part consisted of examining the experimental data obtained from DIC as a means for pre-processing and analysis of the data quality. The second part of the work was concentrated on constructing FE models whose results could be compared to the available experimental data and to calibrate the material models by using an optimising method.

In order to assess the calibration method and how it is affected by different prerequisites, different case studies were carried out. The aim of the case studies was to investigate how different assumptions of the material model and of the FE modelling affected the results and thereby also giving an indication of the calibration method's robustness. This thesis therefore provides an idea of how this calibration method could work and what potential it has by showing some of the potential pitfalls to avoid when developing the method further. Since the developed method is material model independent, more advanced materials and models could be evaluated in the future.

Acknowledgements

Contents

1
Introduction

With Finite Element (FE) modelling becoming more widespread, the importance to have accurate models that can give good predictions increases. This project was created to obtain a method of calibrating FE models using data obtained from Digital Image Correlation (DIC).

1.1 Background

FE modelling is an important component in the product development processes, allowing for the amount of physical testing to be substantially reduced and thereby shortening the lead times during development of new products. In order for the FE models to make accurate predictions, the model parameters must be determined to give a good agreement between the model and the reality. For new materials such as hybrid materials or manufacturing processes such as additive manufacturing this may require the use of novel test procedures. It is therefore of interest to find ways to accurately determine model parameters for different materials and geometries.

To make accurate predictions, calibration of the FE models is a necessity. This is usually performed by using experimental data that can be compared to results from FE simulations. DIC is a non-contact method that uses optical tracking and image registration techniques to measure changes in images. DIC can thus be used to measure displacements on the surface of test specimens [1].

The thesis work has been carried out at the Mechanics Research department at Research Institutes of Sweden AB (RISE). The department works with a broad spectra of services covering testing, quality control, fatigue life assessments, damage investigations and research. With advanced experimental resources and competence in testing, many projects are performed for the industry and for research purposes. In previously performed projects at RISE, DIC has been used to study the mechanical behaviour of materials and components subjected to loading. A significant amount of DIC data available from these projects constitutes the foundation for this work [2].

1.2 Objective

The aim of this project was to obtain and evaluate a method that uses DIC data to calibrate FE models. Quantifying the ability to make accurate predictions will play an important role in the evaluation of the method together with an investiga-

tion of the uncertainties in the procedure and naturally occurring variations in the materials.

1.3 Problem definition

To achieve the objective to calibrate FE models with DIC, the task had to be broken down to smaller portions.

The calibration will require a specification of what it means to be calibrated and a measure of what is required to classify the calibration as acceptable. Since the calibration procedure is based on DIC data, the quality and behaviour of that data are of interest to investigate. An issue to be solved is how to connect information from the DIC measurements to the results from the corresponding FE simulations. Since the FE models are created for this project, some modelling choices have to be made as well.

1.3.1 Material models

Calibration in this case will refer to optimising the agreement between test results and results from calculations with a given material model. The calibration will therefore determine the parameter values in the material model that give the best correlation when comparing results calculated by FE simulations with the corresponding values obtained with DIC measurements. With this approach, the choice of material model will affect how good the correlation between the results from FE simulations and experimental data can become. Considering this, there is a need of quantifying the correlation so that different material models can be compared to choose a good one. In general a more complex model that subsequently uses more information has a potential to give a better correlation between the experimental and the modelled data. There is however a limit for when an increased model complexity does not increase the model's ability to mimic the experimental observations further. There is therefore of interest to investigate how complex a model is required to be to get good correlation while still not being more complex than necessary.

1.3.2 Linking process

To make it possible to identify the parameter values that gives the best fit between the experimental observations and the model output, there needs to be some way of connecting the displacements and load cases known from DIC measurements with the FE models. It is thus of interest how this connection should be made. The term connection includes both the practical part of creating a program routine that can work with the two data sets but also the part of realising what information that is necessary to use for the comparison to make sense.

Figure 1.1 shows the necessary steps to connect the results that are obtained by the experiments and the simulations respectively.
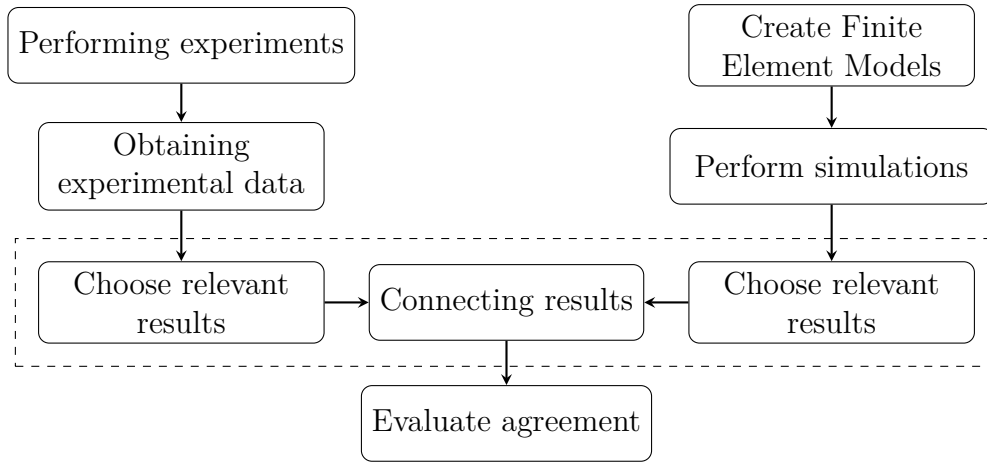
Figure 1.1: A schematic view over the process of linking results obtained from experimental data and results obtained from simulations. The box with dashed lines contains the linking part of the procedure.

1.3.3 Uncertainties and modelling challenges

There is always a risk of errors to occur when considering experimental data and data obtained from simulations. The manufacturing of test specimens, the quality of the measuring systems and the data analysis will all be possible error sources connected to the experimental data. Natural variations in test specimens and noise in experimental data are always present as well.

When creating FE models, simplifying assumptions are necessary. Not only the choice of material model will affect the calibration results, but other parts of the modelling as well. The correctness of the FE model, the meshing and correct interpretation of the boundary conditions are examples of what can affect the calibration. During the calibration there are a risk of errors to occur as well. This could be due to coding errors and what tolerances that are chosen for the optimising routine but also how the comparison of the results are performed. Being careful and thorough when constructing the calibration routine will help to minimise these errors.

1.4 Limitations

There are a fixed number of test specimens that have been monitored during testing using DIC. No additional data collection will be performed during this project, so the material is limited. The DIC measurements have been made with use of the program Aramis and no focus will be put into how the DIC is performed by the program. The predefined set of test specimens limits the base material to steel in room temperature only.

With obtaining the calibration method as the main objective, firstly the calibration will only be based on few parameters and valid for elastic cases. More parameters

and plasticity will be considered only when a working method is present. Since the time did not permit to investigate all models and parameters of interest, those are left as ideas to further development.

2

Computational modelling

This chapter is meant to serve as a help to understand the models upon which the simulations in this project are based on. In particular general concepts of the finite element method, as well as the underlying material models, will be briefly explained. The chapter ends with an introduction to inverse problems and model calibration which will be presented more detailed in chapter 4. The model calibration part is strongly linked to the experimental procedures which are presented in Chapter 3.

2.1 Finite element modelling

Many engineering problems can be represented by mathematical models describing the relevant physics. A majority of these models are based on differential or integral equations. The Finite Element Method (FEM) is a numerical method for approximating the solutions to complex problems that cannot be solved analytically. The solutions obtained by FEM will depend on what mathematical model that is chosen to represent the physical problem [3]. A scheme over how the finite element analysis works on a problem can be seen in Figure 2.1.

2.1.1 Material models

Since the solution obtained by a finite element analysis depends on what mathematical description that is used to model the physical problem, it will only predict results as good as the mathematical model. When it comes to predicting how different materials will behave during loading there are several assumptions that affect which mathematical model to use when representing the material behaviour. The assumptions related to the behaviour of the materials are used in the formulation of a relevant, in relation to its intended use, model.

One assumption to make is whether a material could be considered homogeneous or non-homogeneous. A homogeneous material is pure, without traces from other materials. Most engineering materials are considered to be homogeneous, with composite materials as an obvious exception.

Another assumption to make is whether the material has the same properties in all directions or not. If it does, the material is considered to be isotropic. Most metals are considered to be isotropic, thus they will be assumed to have the same behaviour independently of in which direction the load is applied. As the available test data in this project is taken from samples made of steel, it is assumed that the material behaves homogeneously and isotropic. Transversely anisotropy could be
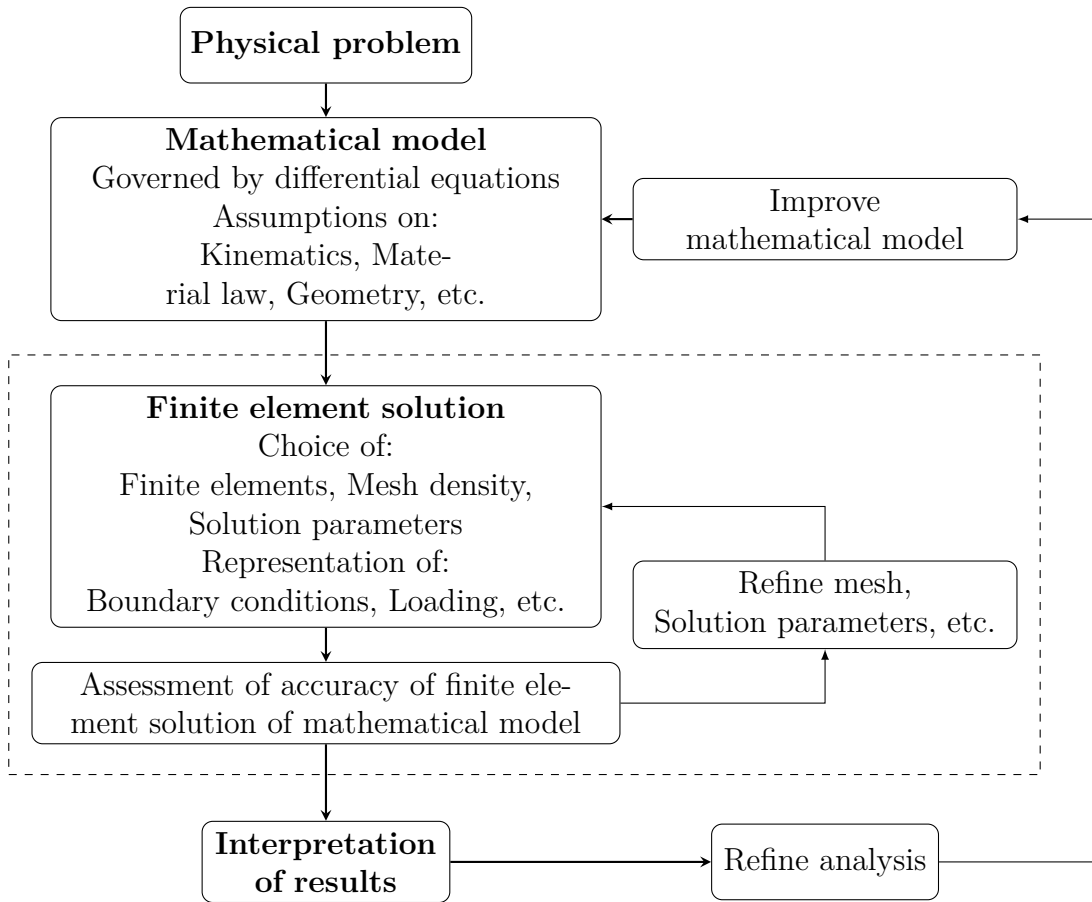
Figure 2.1: The process of the finite element analysis, adopted from [3]. A physical problem is modelled by mathematics which in turn uses different assumptions such as kinematics and material laws. The finite element solution then adds additional choices that have to be made before performing an analysis, such as element types and mesh density. The dashed box encapsulates the process of refining the finite element solution based on a specific mathematical model. After finding an acceptable solution for the mathematical problem, the results can be interpreted and the mathematical model can be subjected to refinement.

possible due to the manufacturing method but here the assumption of isotropy is made to simplify the modelling and the calibration procedure.

Constitutive equations states the relation between two physical quantities that is specific for a material. For structural analyses the constitutive equation of interest is usually the one relating stresses and strains. When referring to material models during this project, it is the constitutive models that is meant. The linear elastic model and a elastic-plastic model with hardening will be explained here since they are considered later.

The linear elastic model assumes that the material will respond in a linear elastic way when subjected to loading. This means that the material will return to its original size and shape when the load is removed. The linear part addresses the linear relationship between the stress and strain and is for isotropic materials called

Hooke's law. This law is assumed to be valid up to the elastic limit for most metals and crystalline materials.

Plasticity is the term describing what happens after reaching the elastic limit. When entering the plastic range the material will no longer return to its initial size or shape when unloaded and permanent deformations will occur. A perfect plastic material will continue to deform as long as the yield stress is maintained. If the stress is reduced the material will unload elastically. It is more common to have some kind of hardening present, where the stress needs to increase for further plastic deformation. If the loading is held constant, the material will neither be elastically unloaded nor will any further deformation occur [4].

The material parameters that are associated to linear elasticity and a linear hardening will be described more carefully in chapter 3.

2.2 Calibration and validation

To validate how good the prediction of an FE model is and to improve the results in the future, experiments can be performed. For the model to be called accurate, the agreement between the model and the experiment should be as good as possible. Improving the mathematical model and more explicitly the values of material parameters will thus be a step to calibrate the model to perform better.

2.2.1 Inverse problem

Here, the concept of inverse problems will be briefly outlined. When working with modelling, the problems encountered can be said to be direct problems or inverse problems. A direct problem would consist in a model structure with a given mathematical model and loading, which is solved by FE analysis to obtain the response of the model.

When the purpose is to calibrate the model, the problem is instead considered to be inverse. Inverse problems differ from direct problems by that instead of having known material and model parameters, the response of the model is known. The response for an inverse problem is obtained by performing some sort of experiment where data is collected. Instead the interest lies in finding the model parameter values that give the best agreement to the results.

A scheme over the flow for the two problem types can be seen in Figure 2.2. For an inverse problem there can be multiple solutions and thereby possibly providing a more complicated problem than the direct problem [5].

Input   **Output**

| Model structure
Loading f
Parameters p | → | Direct solution | → | Response r |

Input   **Output**

| Model structure
Loading f
Response r | → | Inverse solution | → | Parameters p |
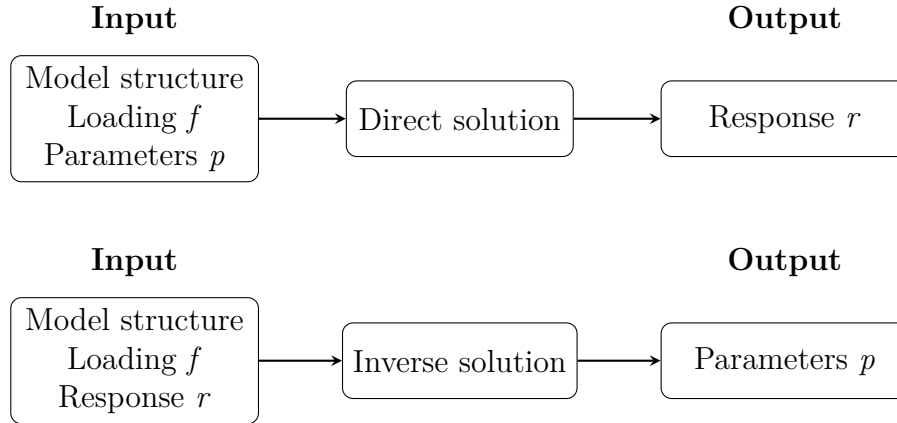
Figure 2.2: A schematic view over the difference between a direct and an inverse problem. For a direct problem, the material parameters of the model are known and the desired output is the response of the model. For an indirect problem, the response of the model is known and the material parameters that result in the given response is sought for.

2.2.2 Parameter identification

To identify the values of the model parameters, different strategies can be used. A graphical, more direct identification of the parameters can be obtained by designing the experiments such that each parameter can be found and physically interpreted. However, that requires the parameters to be uncoupled and it might be hard to construct suitable experiments.

A more general strategy is to use nonlinear optimisation algorithms to determine parameters simultaneously. This requires less from the experimental setup and is a general strategy but can be time consuming and having multiple optima due to incomplete data.

3

Experimental procedure and analysis

With the aim to obtain a general procedure of using DIC for calibration of FE models, the quality and understanding of the data obtained by DIC is of great importance. The first part of the project was therefore dedicated to analysing the DIC data independent of the FE modelling. During this phase, scatter of the data was examined together with a general understanding of how this data could be combined with the FE models in the best way. This chapter will therefore present the testing method, the test specimens that have been used during this project and explain in detail how the data was processed before using the DIC data in the FE calibration.

3.1 Tensile testing

A standard procedure to determine material parameters that can be used for modelling purposes is the tensile test. A common tensile test results in engineering stress-strain data, which means force per unit undeformed area versus length change per unit undeformed length. This is accomplished by letting a test specimen be subjected to a tensile force in a controlled manner [6].

Specific machines exist for this purpose and a schematic figure of a test machine can be seen in Figure 3.1. The test specimen is attached by two holding grips, of which one is attached to a moving crosshead. These grips can have different properties and in this project, a spherical seating was used to prevent any torque or bending moment to arise within the specimen. Test specimens are manufactured according to standards and an example is presented in Figure 3.2. The initial diameter d_0, shown as d in the figure, is measured prior to testing and the initial distance L_0 is known as well. During testing L_0 will be elongated and an extensometer is therefore attached to track the current length L.

During testing, the movement of the crosshead is performed in a controlled manner while a load cell measures the applied force, F. With the known values of L_0, L, F and the nominal radius $r_0 = \frac{d_0}{2}$, the engineering stress, σ, and engineering strain, ϵ, can be calculated according to

$$\sigma = \frac{F}{r_0^2 \pi}, \qquad \epsilon = \frac{L - L_0}{L_0}. \tag{3.1}$$
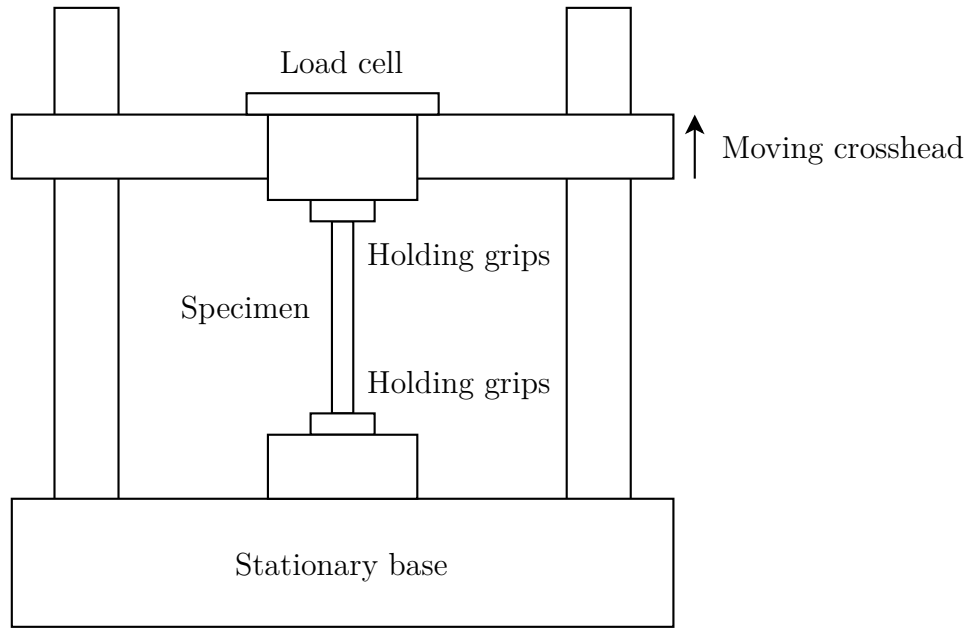
Figure 3.1: The setup of a tensile test. The test specimen is fastened at both ends, one end is kept fixed by the test machine while the other is subject to a controlled force measured by the load cell.
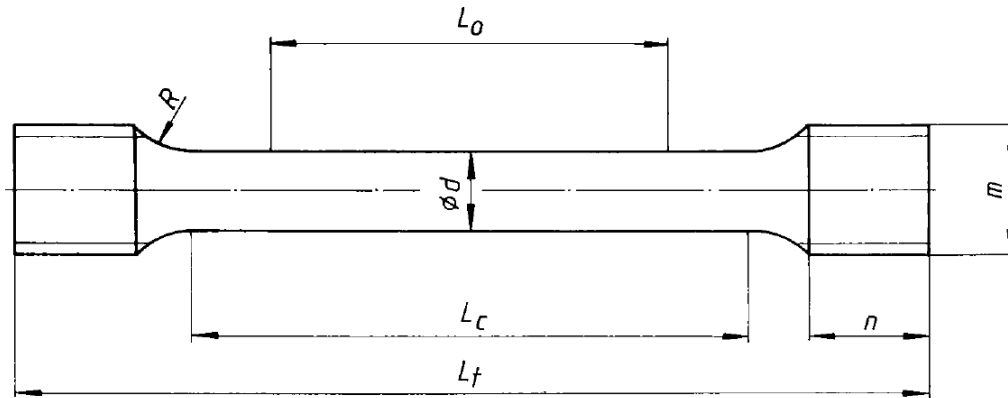
Figure 3.2: A standard cylindrical test specimen [7]. The middle of the specimen is thinner compared to the ends that are attached to the grips, d constitutes the nominal diameter. L_0 marks the part of the specimen that is studied and used for elongation calculations while L_c is the parallel length of the specimen.

Multiple material parameters for the test specimen can then be determined from a stress-strain diagram. Figure 3.3 shows a typical stress-strain curve obtained from one of the samples used later in this project. The curve segment that reaches from the origin to the cross in the figure is called the elastic range of the material. As mentioned during the previous chapter, the stress in this range is assumed to depend linearly on the strain where the elastic modulus, E, is obtained as the proportionality constant. When the stress has reached the so called yield stress, σ_y, the material will not behave linearly anymore and instead enter the plastic range of the stress-strain curve.

Engineering stress-strain curve

Figure 3.3: Typical stress-strain diagram obtained from a tensile test. This one is obtained from test specimen S0_PLATE_A_30_02_A that were used in the project. The cross marks where the elastic range ends.

To obtain the value of σ_y, a common method known as the offset yield method is used [6]. The distinction between the elastic range and the plastic range is not always trivial to find, motivating this method. To find the value of the yield stress a line with a strain offset of 0.2% from the origin is constructed. The slope of this line should be the same as the slope of the elastic interval of the engineering stress-strain curve. The so called offset yield strength, σ_o, is then considered to be the value of σ where the constructed line intersects the stress-strain curve [8] and is often chosen to represent σ_y. An illustration of the method is shown in Figure 3.4. The ultimate tensile strength, σ_u, is the maximum engineering stress that is reached in the engineering stress-strain curve.

When interested in determining material parameters connected to the hardening of the material a curve based on the true stress, σ_{tr}, and true strain, ϵ_{tr}, is useful. The true stress is calculated based on the current smallest radius, r, of the sample instead of the nominal radius. The true strain is based on the incremental length. The expressions for the true stress and true strain are written as

$$\sigma_{tr} = \frac{F}{r^2\pi}, \qquad \epsilon_{tr} = \int_{L_0}^{L} \frac{\mathrm{d}L}{L} = ln\frac{L}{L_0}. \tag{3.2}$$

Engineering stress-strain curve
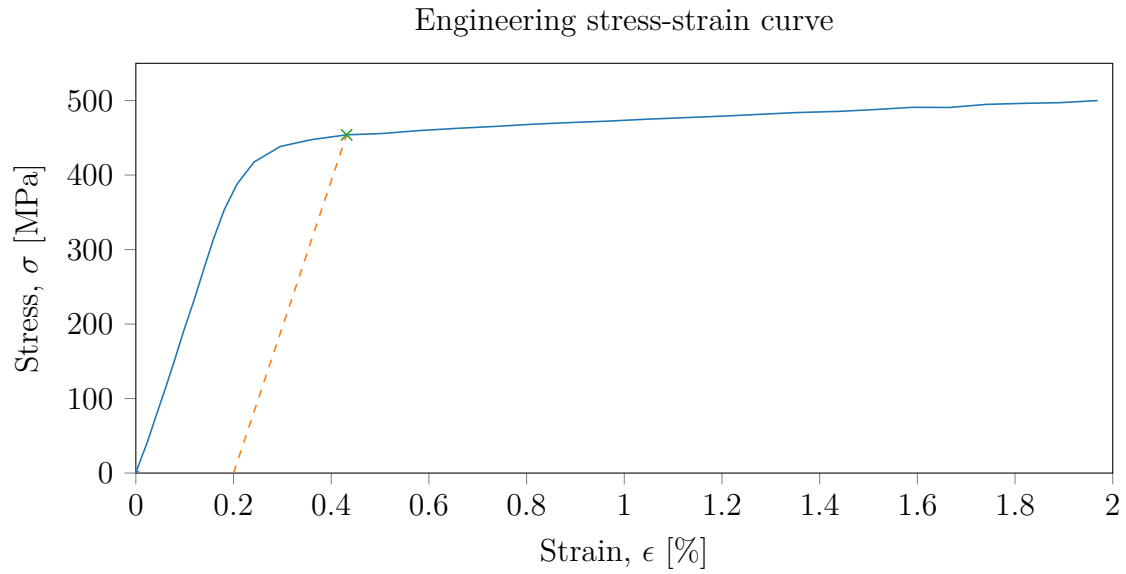
Figure 3.4: The principles of the offset yield method are shown for test specimen S0_PLATE_T_30_02_A. The dashed line is constructed with a strain offset of 0.2 % from the origin and the value of σ at the intersection between the two curves becomes the offset yield strength, here marked by a cross.
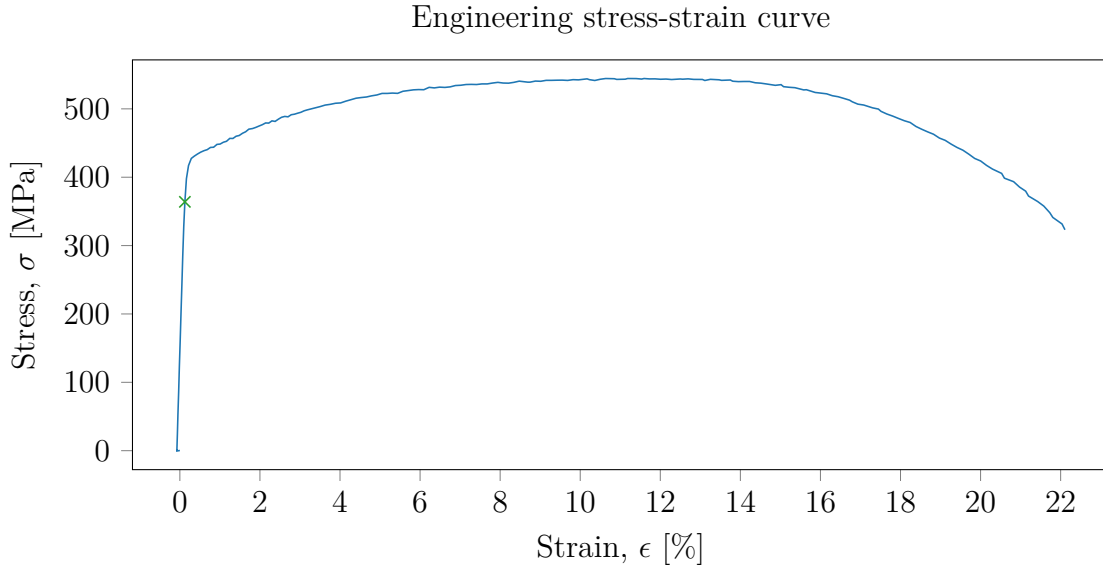
True stress-strain curve
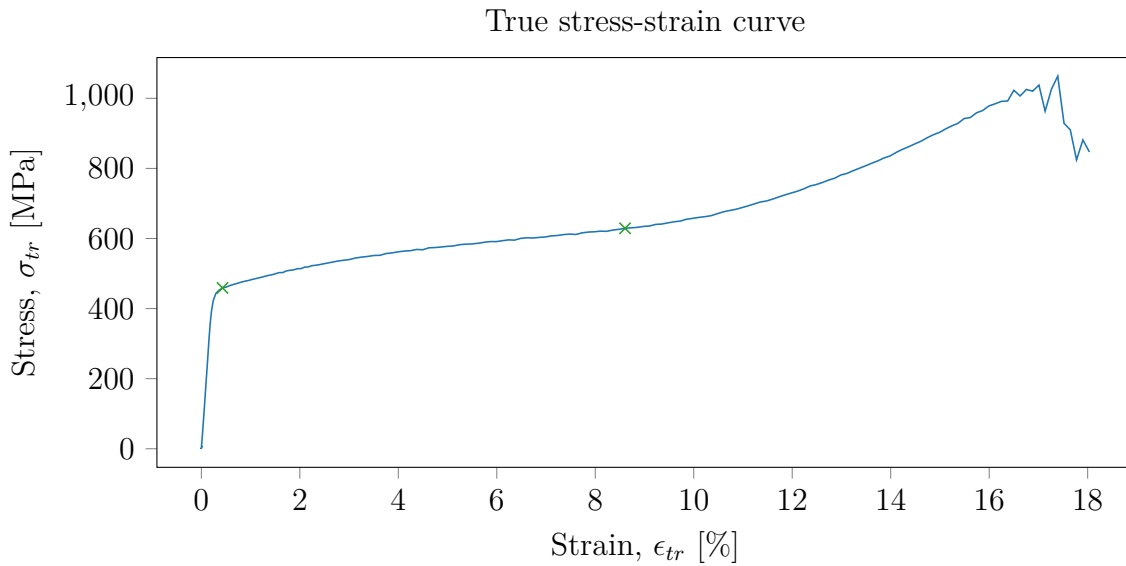
Figure 3.5: Typical true stress-strain diagram obtained from a tensile test. This one is obtained from test specimen S0_PLATE_A_30_02_A that was used in the project. The crosses marks where the offset yield strength and the ultimate tensile strength is found respectively.

A typical true stress-strain curve can be seen in Figure 3.5. A rough approximation of the hardening can be reached by using the slope between the offset yield strength and the ultimate tensile strength from the true stress-strain curve. This approximation

will be used as input when choosing a range in the global analysis of which the results are presented in section 5.2.2. Let $\epsilon_{o,tr}$ denote the true strain at the offset yield strength and $\epsilon_{u,tr}$ denote the strain at the ultimate tensile strength. Then by using the true stresses at those locations, $\sigma_{o,tr}$ and $\sigma_{u,tr}$, a linear hardening parameter, H, can be obtained as

$$H = \frac{\sigma_{u,tr} - \sigma_{o,tr}}{\epsilon_{u,tr} - \epsilon_{o,tr}}. \tag{3.3}$$

It is usually hard to achieve a true stress-strain curve since the radial displacements not always are practically possible to measure during the deformation by the use of conventional methods.

3.2 Digital image correlation

A method to measure displacements while performing tensile tests is by performing DIC. DIC is an image technique based on the ability to track positions of an object in three dimensions and can thus provide displacements in all directions over the monitored domain of the specimen surface. This means that more information about displacements is provided compared to tensile tests, where displacement is only found for distances covered by extensometers.

The correlation works by having two cameras tracking the test procedure. Image analysis is then used to correlate pixels between the two images and by the relative positioning of the cameras be able to determine the three dimensional coordinate of that pixel. Since each pixel is seldom unique a larger region of pixels, so called facet or subset, is used during correlation. For each such facet the position value for each pixel is averaged to apply to the full region. This averaging makes the facet value more stable if a lot of pixels are included, but with increasing size of the facet, the resolution of local displacements is lost. Therefore a trade-off between stability and resolution has to be done for the calculations.

In addition to using facets as a way to make the correlation unique, the surface of the specimen needs to be non-homogeneous to distinguish pixels and facets from each other. This is possible for materials with an in some way irregular pattern that can be used in data analysis to register certain regions. The pattern can be from the object itself or it can be applied later, but has as its purpose to make different parts of the object easier to distinguish, something that would not be possible with a perfectly polished surface.

When used to track a tensile test, the DIC system can be setup as in Figure 3.6. Compared to only performing a standard tensile test, this method provides full-field measurements without having to decide where to locate extensometers.
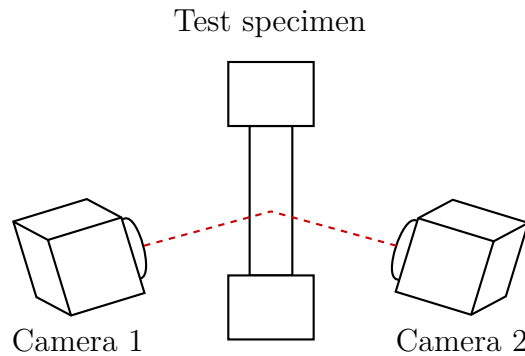
Figure 3.6: The spatial setup of a DIC system while tracking a tensile test. Two cameras record the position of the sample while the tensile test is running. By knowing the relative placement of the cameras and comparing the two images, digital image correlation can then be performed.

3.3 Experimental data acquisition

Experimental data existed from a prior project that RISE conducted during 2017 [2]. This data consists of results from tensile tests performed at RISE:s premises in Borås measured by the DIC system Aramis professional 2016 from GOM. The test specimens and data selection are presented below.

3.3.1 Test specimens

All tensile test specimens used in this project were cylindrical, made of steel and manufactured from plate material. The test specimens were manufactured according to guidelines in EN 10225:2009[9] and the geometry of the cylindrical test specimens is specified by the standard SS 11 21 13[7]. The geometrical parameters of the test specimens were illustrated in Figure 3.2. The diameter of all test specimens was measured at three locations using a micrometer screw.

A list of all tensile test specimens and their dimensions used for this project are listed in Table 3.1. The names of the test specimens are generated based on the features of the specimen. As can be seen in the table all specimen names starts with S0_PLATE, this refers to that all specimens are from Series 0 and made out of plate material. The letter A or T that follows S0_PLATE tells whether the specimen has been extracted along or transverse to the rolling direction of the base plate material. The last part of the name then states the thickness of the plate material that the

specimen was extracted from and a serial number to ensure unique names for all specimens.

Table 3.1: Dimensions of all tensile test specimens used during this project. L_c is the parallel length and d is the nominal diameter while d_{min} and d_{max} are the maximum and minimum diameter measured by the micrometer screw. The listed types are associated to specific values of L_c and d, for the interested reader more information regarding the types can be found in standard SS 11 21 13[7].

Test specimen name	Type	L_c	d	d_{min}	d_{max}
S0_PLATE_A_10_01_A	5C50	60	5	4.95	4.99
S0_PLATE_A_15_01_A	7C70	85	7	6.94	6.98
S0_PLATE_A_20_01_A	10C50	70	10	9.97	10.0
S0_PLATE_A_30_01_A	14C70	100	14	13.97	14.01
S0_PLATE_A_30_02_A	14C70	100	14	13.98	14.02
S0_PLATE_A_40_01_A	14C70	100	14	13.98	14.02
S0_PLATE_T_10_01_A	5C50	60	5	4.97	5.00
S0_PLATE_T_15_01_A	7C70	85	7	6.97	7.01
S0_PLATE_T_20_01_A	10C50	70	10	9.95	9.99
S0_PLATE_T_30_01_A	14C70	100	14	13.97	14.01
S0_PLATE_T_30_02_A	14C70	100	14	13.97	14.01
S0_PLATE_T_40_01_A	14C70	100	14	13.96	14.00

Furthermore, it can be seen that the values measured by the micrometer screw, d_{min} and d_{max}, sometimes are smaller or larger than the nominal diameter d. As part of the standard manufacturing, tolerances are listed and thereby small variations from the nominal diameter are accepted. Since the displacements were tracked by the DIC system, all specimens were applied with speckle patterns. A specimen before and after this application can be seen in Figure 3.7.
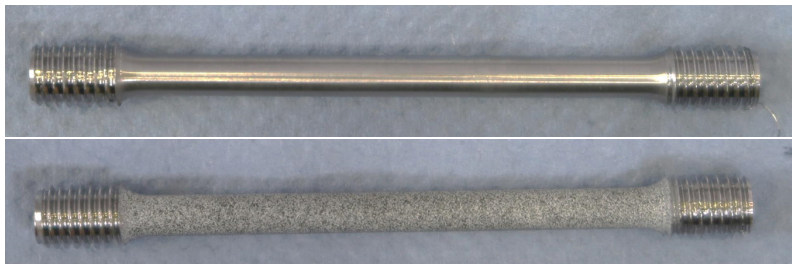
Figure 3.7: Test specimen S0_PLATE_A_10_01_A before and after application of a speckle pattern.

3.3.2 DIC data extraction

The procedure of extracting the relevant DIC data from Aramis was also performed prior to this project but will be explained here to increase the understanding of the DIC data. Each DIC analysis is performed over a certain area that is covered by the cameras. This area will not only include the test specimen but also the space around it. For each sample an area of interest is then chosen together with facet size. An example taken from Aramis can be shown in Figure 3.8. The full image is recorded by the DIC system but only a part of it is chosen as area of interest. Depending on the facet size it is not always possible to fit this choice perfectly, the area that actually will be evaluated is therefore coloured green. Smaller parts of grey can be seen around the green area, those correspond to the area that was chosen but could not fit any facets. For the area covered by facets, the positions, displacements and strains are calculated by Aramis and can be printed to reports. The x-, y-, z-coordinates and the information regarding time steps and applied load are the entities that have been used during this project.
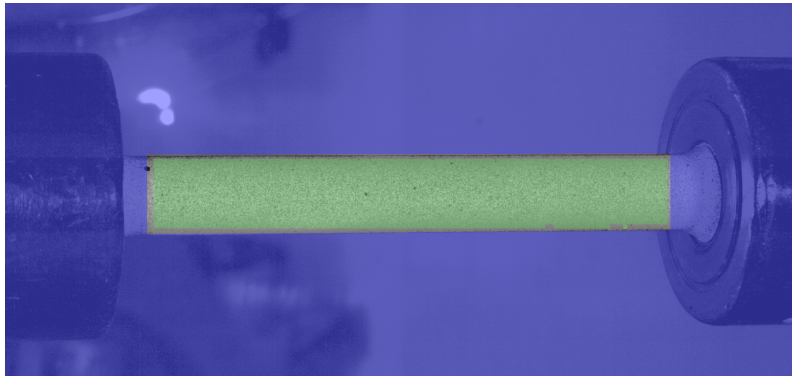
Figure 3.8: The appearance of a test specimen when surveyed in Aramis. The area covered by facets and thus used for analysis is marked green. Image courtesy to Torsten Sjögren.

3.4   Axisymmetric fitting

While performing the tensile tests, the specimens were attached in a way to avoid bending moment from acting on the specimen. A consequence from this was that rigid body motions occurred for some specimens if they were not perfectly aligned when the load was applied. To be able to couple the results from the DIC data to FE models later on, this rigid body motion had to be addressed.

Since the tensile test specimens were all cylindrical a local cylindrical coordinate system attached to the test specimens became the solution for easier coupling. As long as the tensile tests are considered, this solution will provide easier input to the FE models. To get a better understanding of how the data points are located relative to the test sample a fundamental sketch is shown in Figure 3.9 together with a local cylindrical coordinate system. As is shown in the figure, the data points are located in a regular grid aligned with the local coordinate axes of the specimen, covering approximately 100° of the cylinder mantle.
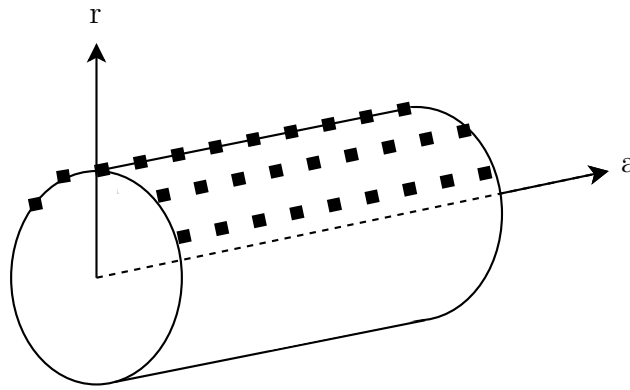
Figure 3.9: An example showing the general appearance of a test specimens and how the DIC data points are located on the mantle area. A local cylindrical coordinate system is attached to the specimen with the centre line of the specimen coinciding with the axial coordinate axis of the system.

To obtain a local coordinate system aligned with the DIC data points a method to find this system had to be found. The first attempt to find a local coordinate system was based on the assumption that all data points were supposed to lie on a cylindrical surface, and the local coordinate system would be the one where the deviation from this cylindrical surface would be as small as possible. During this work it was discovered that the radius varied over the length of the specimen, thus not forming a perfect cylindrical surface. This resulted in a poor fit when trying to obtain local coordinate systems for the specimens. Since this approach did not result in a satisfying result, it will not be explained further in this chapter. Instead another method that allows the radius to vary over the sample length was used. The concepts on which this method is built on will be explained below.

3.4.1 Coordinate systems and transformations

A local coordinate system with one coordinate axis coinciding with the symmetry line of the assumed axisymmetric test specimen can be obtained by a rotation and translation of the original Cartesian coordinate system. The original Cartesian coordinate is given by Aramis with the coordinate axes E_1, E_2 and E_3. This original coordinate system is similar to the local coordinate system that is found by the method described below. The original system is however not following the specimens movements and therefore becomes misaligned over time. That a specimen is axisymmetric is a necessary assumption to make since the available DIC data does not cover the full area of the specimen but this area needs to be modelled later. The task was thus to find how much the current coordinate system should be rotated and translated to make the E_1-axis to coincide with the local axial coordinate axis, a in Figure 3.9. The definition of best fit was changed from the initial assumption to instead emphasise the importance of axisymmetry by minimising the radial deviation for each axial increment along the symmetry line a.

The rotation of a coordinate system is often described by Euler angles, which describes multiple rotations around single axes performed in a sequence, thus resulting in an arbitrary rotation. To achieve the desired rotation and translation mentioned earlier, the movements shown in Figure 3.10 were used. As can be seen in the figure, the two Euler angles α and β will constitute the necessary rotation of the system while the translation is given by the constants C_2'' and C_3'' in the rotated system.
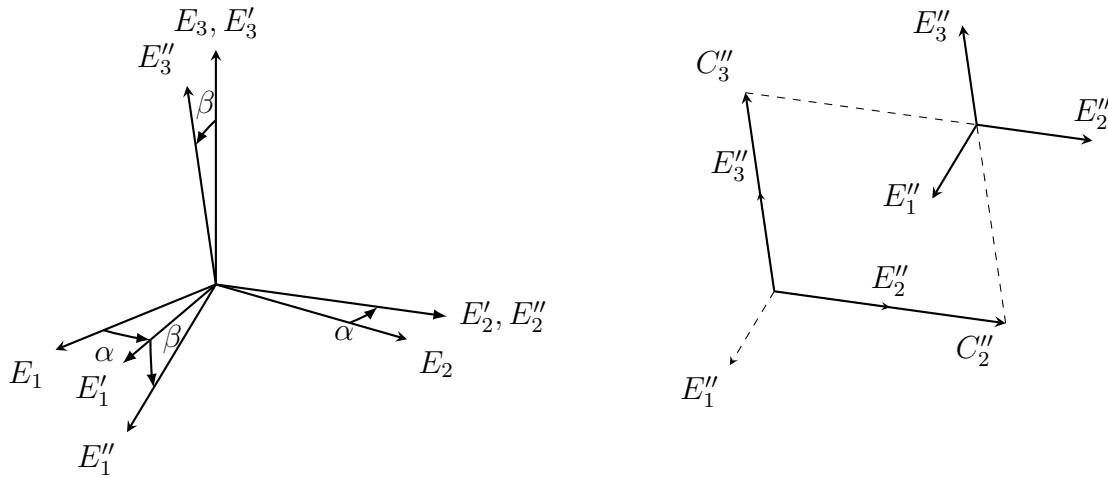
Figure 3.10: The Euler angles α and β rotates the original Cartesian coordinate system to make the E_1''-axis parallel to the symmetry line of the test specimen. The constants C_2'' and C_3'' then gives the distance to move along the E_2''- and E_3''-axes to finally make the E_1''-axis coincide with the local axial coordinate axis, a, of the test specimen. Note that the origin of the local coordinate system is not guaranteed to be located at one of the sample ends by this transformation.

A rotation matrix that can be applied to all coordinates from the initial coordinate system is obtained from equation 3.4 where the two Euler rotations are performed. E_1, E_2 and E_3 are the coordinate axes in the original coordinate system, E_1', E_2' and E_3' are the coordinate axes after rotating α degrees around the E_3-axis and lastly E_1'', E_2'' and E_3'' are the coordinate axes after rotating β degrees around the E_2''-axis.

$$
\begin{pmatrix} E_1' \\ E_2' \\ E_3' \end{pmatrix} = \underbrace{\begin{bmatrix} \cos\alpha & \sin\alpha & 0 \\ -\sin\alpha & \cos\alpha & 0 \\ 0 & 0 & 1 \end{bmatrix}}_{R(\alpha)} \begin{pmatrix} E_1 \\ E_2 \\ E_3 \end{pmatrix}, \quad \begin{pmatrix} E_1'' \\ E_2'' \\ E_3'' \end{pmatrix} = \underbrace{\begin{bmatrix} \cos\beta & 0 & \sin\beta \\ 0 & 1 & 0 \\ \sin\beta & 0 & \cos\beta \end{bmatrix}}_{R(\beta)} \begin{pmatrix} E_1' \\ E_2' \\ E_3' \end{pmatrix} \Rightarrow
$$

$$
\begin{pmatrix} E_1'' \\ E_2'' \\ E_3'' \end{pmatrix} = R(\beta)R(\alpha) \begin{pmatrix} E_1 \\ E_2 \\ E_3 \end{pmatrix} \Leftrightarrow \begin{pmatrix} E_1'' \\ E_2'' \\ E_3'' \end{pmatrix} = \begin{bmatrix} \cos\alpha\cos\beta & \sin\alpha\cos\beta & -\sin\beta \\ -\sin\alpha & \cos\alpha & 0 \\ \cos\alpha\sin\beta & \sin\alpha\sin\beta & \cos\beta \end{bmatrix} \begin{pmatrix} E_1 \\ E_2 \\ E_3 \end{pmatrix}
$$

$$(3.4)$$

3.4.2 Optimisation of symmetry line

The optimal local coordinate for each time step is thus obtained by finding the combination of α, β, C_2'' and C_3'' that gives the minimum radial deviation for each axial increment along the E_1''-axis.

More specifically this is made by calculating the $x''y''z''$-coordinates along the E_1''-, E_2''- and E_3''-axes based on the xyz-coordinates in the $E_1 E_2 E_3$-coordinate system. First calculation is based on an initial guess of α, β, C_2'' and C_3''. The cylindrical coordinates r and a are then obtained for all data points as $a = x''$ and $r = \sqrt{y''^2 + z''^2}$. Since the data points are placed in a somewhat regular grid, as was seen in Figure 3.9, each column of this grid corresponds to a value along the E_1''-axis and thus an axial value. For each column the mean, μ_r, and standard deviation, σ_r, of the radial value for those points can be evaluated. The coefficient of variation $c_v = \frac{\sigma_r}{\mu_r}$ are thus obtained for all axial increments along the specimen length.

The overall deviation is then computed by integrating the coefficients of variation over the specimen length. This value is minimised by letting an optimising routine update the guess of α, β, C_2'' and C_3''. When the smallest value is found, the optimum local coordinate system is considered to be found. For the optimum combination of of α, β, C_2'' and C_3'', the calculated μ_r and mean axial value, μ_a, for each column are used as the resulting cylindrical coordinates. From here on, it is thus these values that are referred to when mentioning the radius or axial value of the specimens. The axisymmetric fitting is performed for each time step individually so that the coordinate system follows the specimen over time.

3.4.3 Analysis of DIC data

As discovered earlier the radius of the test specimens was not constant over the length of the sample. To exemplify this variation, two images of radius as a function of specimen length are shown in Figure 3.11.
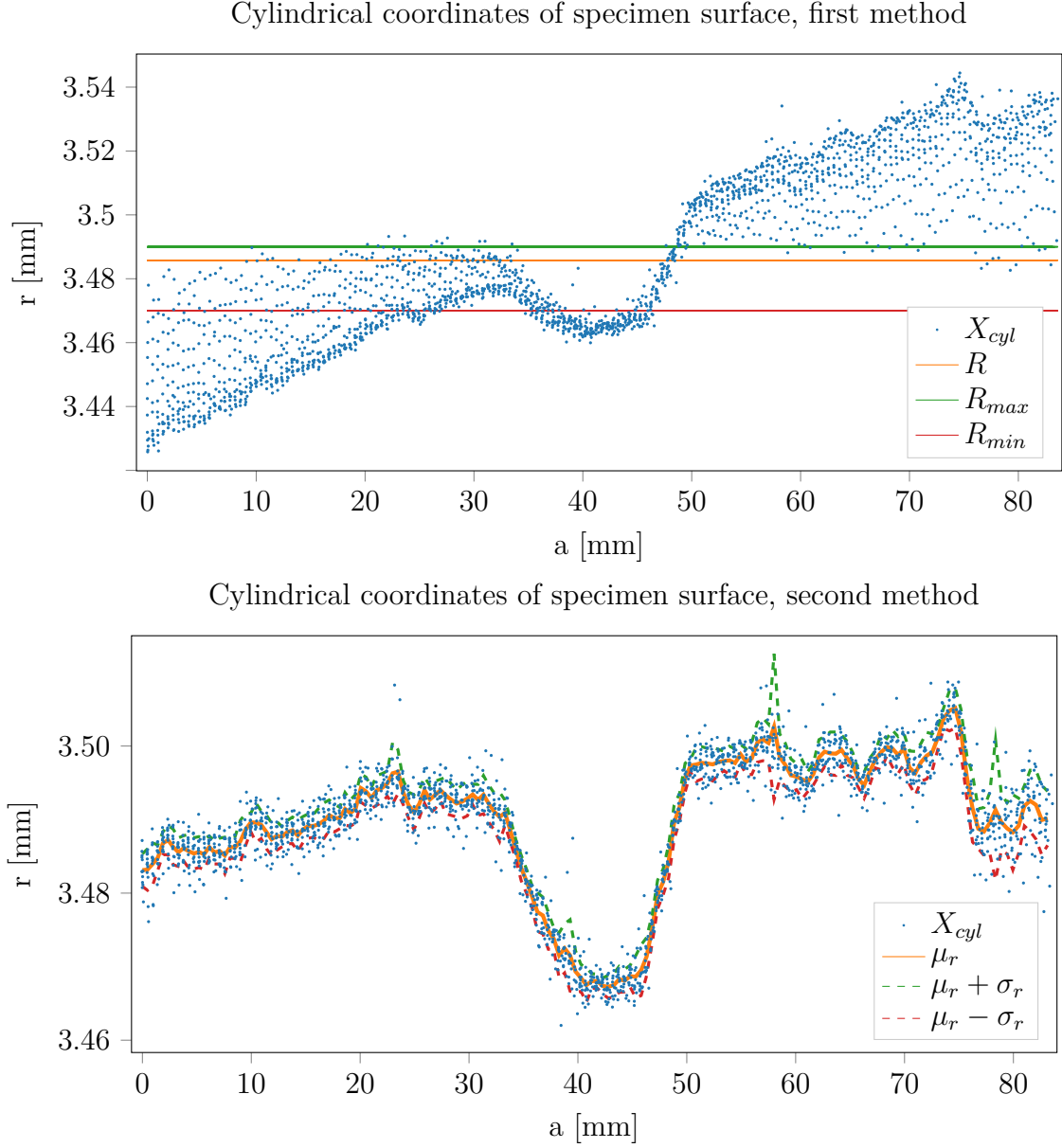
Figure 3.11: The top figure shows the coordinate values, X_{Cyl}, obtained from the first cylindrical fitting method together with the assumed radius of the cylinder, R, and the limits R_{max} and R_{min} that were measured by the micrometer screw. The bottom image shows the coordinate values, X_{Cyl}, obtained from the final method that assumed axisymmetry. The calculated mean radius for each axial increment, μ_r, is shown by itself and with the standard deviation, σ_r added and subtracted to it. Both figures are obtained from test specimen S0_PLATE_A_15_01_A before any load is applied.

The top figure is acquired when using the first method to define a local coordinate system while the bottom figure shows the results when using the second method. The coordinates obtained by the first method demonstrates the problem that occurs when assuming a constant radius. Since there are no radius that fits all points, the method compensates with misalignment of the E_1''-axis compared to the actual a-axis. The misalignment of the axis results in large scatter of the calculated coordinates around the ends of the specimen which also gives a non-axisymmetric representation of the specimen. As can be seen in the bottom figure, the scatter is highly reduced with the second method, which is interpreted as good correspondence to axisymmetry.

In addition to the improvement between the two methods and the varying radius, other interesting things can be concluded from this example as well. The varying radius seemed strange at first but later on seemed more reasonable. When samples are manufactured according to standard they are turned to achieve the rotation symmetry, thus axisymmetry is most likely obtained while a total fix radius is more complicated to achieve. To make it more predictable where the necking will occur, it is during manufacturing possible take advantage of the allowed tolerance to make the cylinder a little bit thinner around the middle. The manufacturing method can thus motivate the assumption of axisymmetry and also explain why a drop in radius around the middle is visible for most specimens.

The measured limits, R_{max} and R_{min}, are the maximum and minimum radius that were measured by the micrometer screw. Ideally, all coordinate values ought to be within that range but as was seen in the top of Figure 3.11 this was not the case. Possible explanations for this could be the fact that the diameter is only measured at three locations over the specimen, according to standard, which could mean that more diameter samples could have given a larger interval. For many samples the radial values, μ_r, in general seems to lie in the upper range of the measured interval or above the measured dimension limit. This could be related to the fact that the specimens are measured before the speckle pattern is applied. Since the magnitude of the radial variance is small, even a thin layer of colour could make a difference. No measurements were made on the specimens after the paint was applied.

The value of adjusting the coordinate system was, as mentioned earlier, a way to make the data easier to compare with results from FE modelling.

An example of how the specimen is being subjected to rigid body motion can be seen Figure 3.12, which shows the Euler angles over time for test specimen S0_PLATE_A_10_01_A.
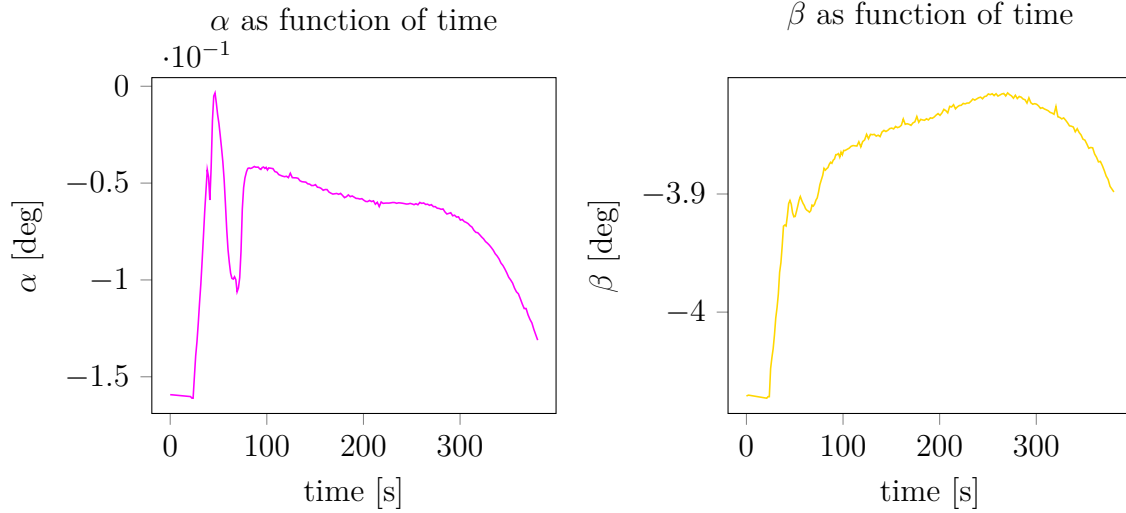
Figure 3.12: The two Euler angles, α and β, plotted over time for test specimen S0_PLATE_T_30_01_A. As can be seen the angles vary most in the beginning, corresponding to rigid body motions of the test specimen when the force is applied.

As can be seen in the figure the angles vary most at the beginning, corresponding to rotations of the specimen, and then stabilises. This demonstrates the rigid body motion that the specimen undergoes when the force is first applied. Even though the value does not change a lot, a misalignment of 0.1° would cause a relative displacement around 0.1 mm. Compared to the order of magnitude in the variation of the radius, which is 0.01 mm it is ten times this value, which validates the need of finding a local coordinate system.

3.4.4 Estimating material parameters

When cylindrical coordinates were obtained for the test specimens, these were used to estimate material parameters that could be used as reference points when initiating the modelling. The engineering stress and strain and the true stress and strain were all calculated according to section 3.1. The full range of the specimen that was captured by Aramis was used as L_0 and L corresponded to the value of the maximum axial coordinate value. The mean of all radial coordinates from the first time frame was used as the nominal radius, r_0. The current minimum radius that was needed for the evaluation of true stress was obtained as the minimum radius, which means the minimum value of μ_r, for each time frame. The estimations of the material parameters will be presented and discussed in section 5.1.1 and 5.2.1 respectively.

3.4.5   Conclusions to bring into the modelling

From the data analysis some things will be utilised or investigated further when performing the modelling in Abaqus.

The cylindrical coordinates and the assumptions of which they are based on will be implemented in the modelling and calibration phase. More specifically the coordinates will be used in the construction of the model to get as good simulations as possible, how they are used is presented in section 4.1.

It is of interest to investigate the impact of using more information while creating the models. Hopefully a more accurate geometry will result in early prediction of the necking area, the results from this investigation is presented in section 5.3.

The calculation of the cylindrical coordinates are built on the assumption of axisymmetry so along with the knowledge of the varying radius, axisymmetry will be used in the modelling. The assumption of axisymmetry is further strengthened by the manufacturing method of the test specimens.

From the calculations of stresses and strains, suggestions for reasonable parameter intervals were obtained. The true stress and strain diagrams have also supplied suggestions for reasonable parameters to use for the modelling of linear hardening.

4

Model calibration

After obtaining a better understanding of the experimental data, the second part of the project consisted in performing the FE modelling and to calibrate the material parameters based on the experimental data. The primary goal of this part was to obtain a procedure that could take basic inputs for variables such as elastic parameters and number of elements. This procedure is then supposed to be updated to include more sophisticated material models and to introduce validation methods. This chapter is therefore dedicated to the explanation of how the FE models were constructed and how the calibration procedure was made. When a working procedure was established, some test cases were performed to indicate strengths and weaknesses of this calibration method. Those cases and the obtained results will then be presented in Chapter 5.

4.1 Finite element model construction with Abaqus script

The calibration method sought in this project is aimed to be general and thus be applicable to many similar simulations, therefore a generic parameterized finite element model was developed for this purpose. The commercial software Abaqus/CAE 6.16-1 with the finite element solver Abaqus/Standard was used together with its own scripting interface, Abaqus Scripting Interface, to accomplish the task. Due to the similar nature of the specimens, a default script could handle the things common for the models. This section describes the FE simulation procedure with respect to material modelling, choice of element types and meshing. A more detailed explanation of how the Abaqus scripts for model setup works can be found in Appendix A, the scripting structure is based on the structure in [10].

4.1.1 Shape and symmetry

All test specimens are assumed to be axisymmetric with a varying radius as discussed during the DIC data analysis in section 3.4.5. As a result of this, the model is built to be axisymmetric in Abaqus. The contour of this axisymmetric test specimen is built by a sketch whose contour is determined from the initial radius and initial axial positions obtained by the DIC analysis. Thereby the actual radius and not the nominal radius is used when designing the specimens. Each sample thus get an unique contour based on the DIC measurements.

4.1.2 Material model and analysis type

For the initial model setup, only respect to elasticity and a linear hardening model are taken, therefore a general static analysis is used. This choice needs to be reconsidered when more complex material models are used.

4.1.3 Elements and mesh

In Abaqus, continuum elements are used for linear static analysis and for non-linear analyses such as plasticity and geometric non-linearity. A continuum element thus fits for the calculations that are made during this project. Since the problem is also axisymmetric, the element type CAX4R is used. It is a four-node, bilinear axisymmetric quadriliteral which uses reduced integration and hourglass control [11].

The mesh is constructed by seeding the edges of the model and then mesh the specimen from that. The mesh is constructed as structured quadriliterals to maintain control over how the elements appear. An example of how the mesh looks like can be seen in Figure 4.1 which shows a mesh setup for sample S0_PLATE_A_40_01_A.
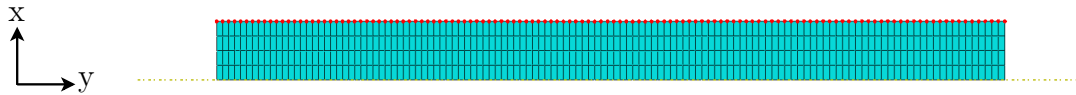
Figure 4.1: Test specimen S0_PLATE_A_30_02_A when using a mesh with 4 elements in the radial direction and one element for each of the specified nodes. The nodes that were specified by coordinates from the DIC analysis are marked red.

4.1.4 Boundary conditions

To get a correct comparison, the FE model should mimic the setup that was used when collecting the DIC data. As the DIC data only corresponds to the gauge part of the tensile test, only this part was modelled in Abaqus. The radial coordinates corresponds to Abaqus x-axis while the axial coordinates corresponds to Abaqus y-axis. The boundary conditions are illustrated in Figure 4.2.
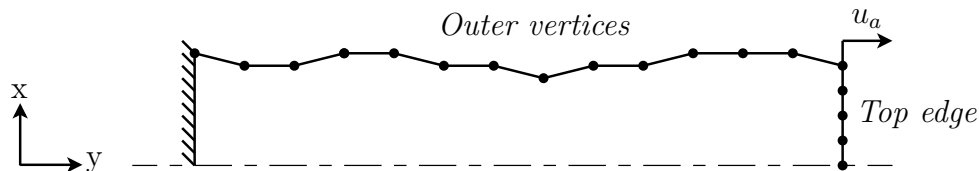
Figure 4.2: Boundary conditions that were used for the models. One end of the test specimen was kept fixed, while the other end had a prescribed displacement in the axial direction. The set *Outer vertices*, includes all nodes that are specified from the DIC coordinates and set *Top edge* includes all nodes on the moving edge of the specimen.

The end where y=0 was kept fix in the y-direction and the other end had y being controlled by a given displacement, u_a. The magnitude of this displacement was obtained by using the corresponding value obtained from the DIC analysis. Time steps were created in Abaqus to correspond to the different time frames in the DIC analysis, thus changing the magnitude of the boundary condition in each time step. Along the symmetry line where x=0, a symmetry boundary condition was used. This condition locks the displacement in the x-direction and prevents rotation around the y- and z-direction. The point (0,0) was kept as a reference point and was thus kept fixed. The surface of the specimen was free to move.

4.1.5 Set creation and result output

To easily obtain displacements from the nodes associated with the DIC measuring points, sets were created for the model. One set included all nodes that were specified from DIC coordinates, which means the nodes on the model surface. This set is called *Outer vertices*. For all analyses performed during this project this is the same as all nodes on the surface. Fore a later version it might be of interest to interpolate between data points and then not have direct correspondence between surface nodes and data points. Another set includes all nodes at the end of the specimen where the displacement is prescribed. This set is called *Top edge*. Both of these sets were shown in Figure 4.2.

After running an analysis job in Abaqus, results are extracted for the two sets. The displacements $u_1 = u_r$ and $u_2 = u_a$ are obtained from the *Outer vertices* set while reaction forces F are obtained from the *Top edge* set. Together with timestep and node number they are written to report files that can be read easily outside of Abaqus.

Since the vertices in the set *Outer vertices* corresponds to the DIC coordinates, the displacements obtained by the FE analysis can be directly compared to the displacements available from the DIC data. The sum of the forces obtained from the set *Top edge* can similarly be compared directly to the registered force that was applied by the test machine.

4.2 Calibration of model by coupling of DIC data with FE results

What has been described above is the setup that the Abaqus script performs when called upon. The shape of the specimen and the applied load are depending on what sample that is considered while the mesh and material parameters should be possible to alter when trying to optimise the fit between the measurements and simulation. Optimisation in general usually refers to maximising or minimising some aspect of a problem, called the objective. For this case of calibrating FE models, force and displacement data are known from experiments and simulations. The desired objective thus becomes to minimise deviations between these values.

4.2.1   The objective function

The magnitude of the deviations are affected by the material parameters that the simulations are built on. If the material parameters are denoted $\mathbf{p} = (p_1, p_2, ..., p_m)$, the displacements of all nodes and reaction force at the end of the sample can be written as $\mathbf{u}_{1sim}(\mathbf{p})$, $\mathbf{u}_{2sim}(\mathbf{p})$ and $F_{sim}(\mathbf{p})$ to emphasise the dependence of the material parameters. The experimental data is denoted as $\mathbf{u}_{1exp}$, $\mathbf{u}_{2exp}$ and F_{exp} and do not depend on the material parameters. $\mathbf{u}_1$, $\mathbf{u}_2$ and F for both experiments and simulations also depends on time and potentially multiple experiments.

Let the time entries be written as t_n where $n = 1, 2, ...N_t$ are the number of time entries and $\mathbf{X}_k$ hold all data from a single experiment where $k = 1, 2, ...N_X$ are the serial number of the experiment. Then a more extensive representation would include t_n and $\mathbf{X}_k$ as parameters, as for example $\mathbf{u}_{1sim}(\mathbf{X}_k, t_n, \mathbf{p})$.

Since it is the difference between experimental data and simulations for the three entities $\mathbf{u}_1$, $\mathbf{u}_2$ and F that is of interest to minimise. The differences are also called residuals, with common notation R, and are calculated according to

$$R_{\mathbf{u}_1} = (\mathbf{u}_{1exp}(\mathbf{X}_k, t_n) - \mathbf{u}_{1sim}(\mathbf{X}_k, t_n, \mathbf{p}))^2 \tag{4.1}$$

$$R_{\mathbf{u}_2} = (\mathbf{u}_{2exp}(\mathbf{X}_k, t_n) - \mathbf{u}_{2sim}(\mathbf{X}_k, t_n, \mathbf{p}))^2 \tag{4.2}$$

$$R_F = (F_{exp}(\mathbf{X}_k, t_n) - F_{sim}(\mathbf{X}_k, t_n, \mathbf{p}))^2. \tag{4.3}$$

With these residuals, the objective function could be chosen in a least squares manner as

$$f(\mathbf{p}) = \sum_{k=1}^{N_X} \sum_{n=1}^{N_t} w_{u1} R_{\mathbf{u}_1} + w_{u2} R_{\mathbf{u}_2} + w_F R_F \tag{4.4}$$

where w_{u1}, w_{u2} and w_F are possible weights. The best correlation between the experimental data and the simulated data will then be found when the objective function takes its smallest value. The weight parameters are included since the different terms might have vastly different size and thus contributing to the total objective function unequally. In this project the weights will only be set to 1 or 0, when enforcing more complex material models the weights will have to be more carefully determined.

One issue to consider during this procedure is that the coordinates from each experiment might not be the same as in the model. This can be solved either by extrapolation of the values or as in this case, the model is forced to use the same coordinates as were obtained from the experiments.

4.2.2   Implementing the objective function

Up to this point, the DIC data has been examined and key features have been used as input to a model in Abaqus. A default script that setups the FE model and simulation before running it has also been constructed. With the knowledge about the objective function, the time has come to connect all this. To coordinate the altering of setup files with comparison of results for several setups, a script was constructed in Python. Python 2.7 was chosen as the programming language since Abaqus scripts were built on Python and thus overall Python knowledge was needed

in the project. The overall process of how the script is working is pictured in Figure 4.3.
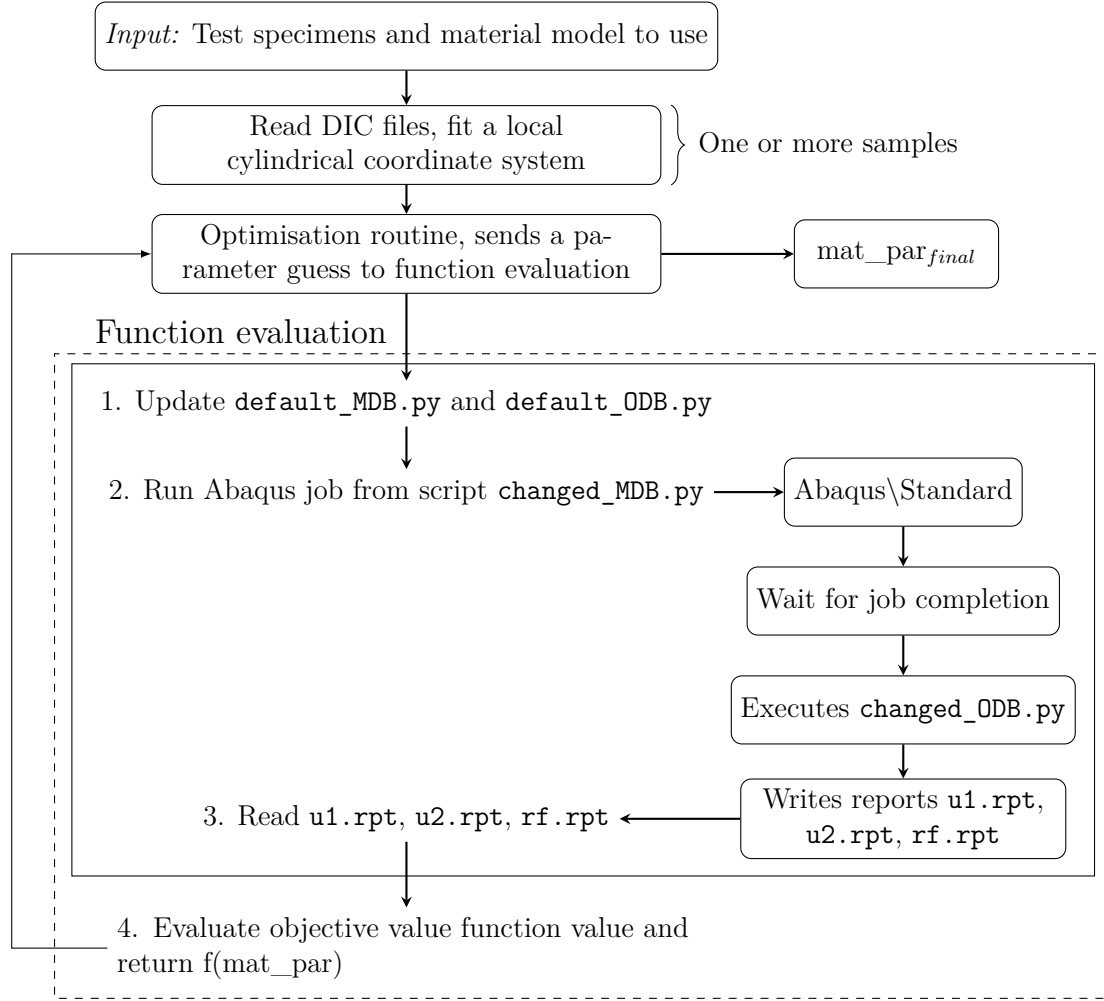
Figure 4.3: Scheme over the calibration methodology. The user specifies what specimens and material model that are to be used during the calibration. The DIC data is then read for the chosen samples and their cylindrical coordinates are determined. An optimisation routine is then used to send in multiple versions of material parameters into function evaluation and iterate until a given tolerance is met.

The scheme can be divided into what is included in the dashed box and what is not. The boxes outside of the dashed box are mainly input values, preprocessing of the DIC data and determination of whether an optimisation routine or only single evaluations of the correlation will be performed. Inside the dashed box the function evaluation occurs, which explains how the correlation for a specific case is calculated. The input given to the program is which test specimens and what material model to use during the calibration. From that choice, the DIC files associated with the test specimens are sent to a preprocessor. The preprocessor determines the cylindrical coordinates and calculates the displacements for each time frame. Before entering the function evaluation an optimisation routine can be applied. If this is the case,

the routine handles what material parameters that should be used in the function evaluation. The choice of material parameters could also be chosen manually and let the user specify material parameters of interest.

With given test specimen, material model, number of elements and material parameters the function evaluation can be carried out. The default Abaqus scripts, `default_MDB.py` and `default_ODB.py`, that controls model creation and result exporting are rewritten to match the desired settings and parameters, thus becomes `changed_MDB.py` and `changed_ODB.py`.

After the scripts have been changed, the Python script tells Abaqus\Standard to run `changed_MDB.py`. Without opening the GUI the model is created and the job is performed. As the scripts `changed_MDB.py` and `changed_ODB.py` are coupled, `changed_ODB.py` executes when the job is completed and writes the reports. When the reports are written by Abaqus, the Python script reads those results. Up to this point the function evaluation has also belonged to a box, this box marks that this can be made for multiple test specimens. When exiting this box the objective function will be evaluated. If an optimisation routine is used, the function value will be compared to earlier results and either be satisfied or try more parameter setups before finally reaching mat_par$_{final}$.

4.2.3 Minimise deviation with global parameter matrix

One approach to increase the probability to find a global minimum is to specify the admissible parameter values and a given set of initial values for each parameter. The objective function is then evaluated for all parameter combinations of the given sets. The best result can be used as an indicative value or as an initial point in a local minimisation algorithm. If only considering two material parameters, the evaluation points can be visualised in a grid similar to Figure 4.4.
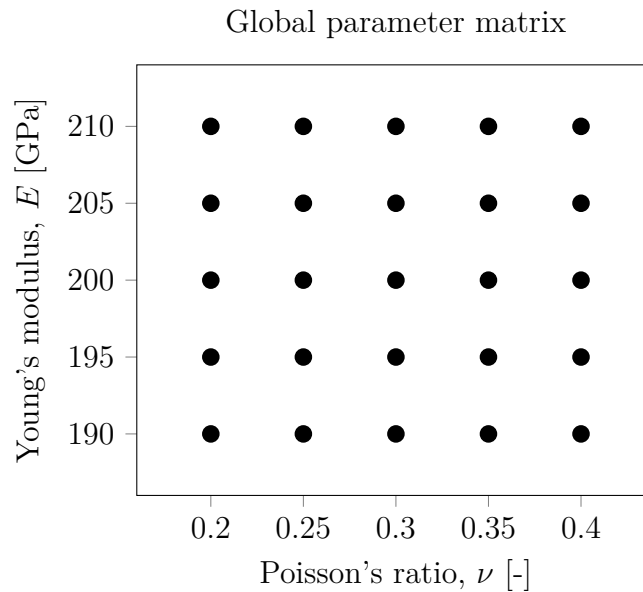

Figure 4.4: Visualisation of a global parameter matrix, the function value is calculated in all points that belongs to the chosen parameter sets.

To determine how the objective function performed and get an overview over the parameter space a global investigation were performed both when estimating the elastic parameters E and ν, and when estimating the plastic parameters σ_o and H. The investigation was performed for all samples, one at a time.

4.2.4   Minimise deviation with optimisation routine

For optimisation of Young's modulus, an optimisation routine was used as well. This was in order to obtain a more accurate value than by the global parameter matrix. This could also have been accomplished by keep refining the parameters in the global parameter matrix manually, but it was of interest to use an optimisation routine as a mean for later purposes when a global parameter matrix cannot provide sufficient information. In this project the Nelder-Mead, also known as downhill simplex method, was used for optimisation purposes. The Nelder-Mead method is a non-gradient method, thus only using function evaluations to determine the local minima. To reach the minima the function is evaluated for $m+1$ points, where m is the number of parameters. These points describes a simplex in the parameter space and for each update the point resulting in the highest function value is replaced by its reflection through the centroid of the remaining m points. The points will keep changing until a converge condition is met [5]. In Python this is achieved by using the `fmin` function from the SciPy package[12]. To see if the results from the Nelder-Mead based optimisation routine was sensitive based on the initial guess, both the best result from the global parameter matrix and the suggestions from the DIC analysis were used as initial guesses in the routine.

5

Calibration results and discussion

This chapter will present and discuss results based on the theoretical framework outlined in Chapters 2-4. Results will be presented for three case studies. The first case considers a linear elastic model and then performs an estimation of material parameters based on DIC data followed by a global estimation and calibration of those parameters. The parameter values that were obtained are presented and reflected on. The second case adds the assumption of plasticity with linear hardening to the model. Similar to the elastic case an estimation based on the DIC data is performed initially followed by a global estimation of those parameters. The third case instead focuses on the determination of fracture location that is obtained based on the DIC data. Lastly there will be a discussion regarding how averaging of data could be a possible help to generate better results.

5.1 Case 1: Estimation of elastic parameters

The simplest material model to assume is the isotropic linear elastic one, this was thus used as the first case. This section will go through the results for the two material parameters E and ν that were obtained when analysing the DIC data and when using the DIC data to calibrate the FE models.

5.1.1 Initial estimation based on DIC data

The engineering stress as function of engineering strain was calculated based on the DIC data associated with each individual test specimen. As an example, the engineering stress-strain curve from sample S0_PLATE_A_10_01_A can be seen in Figure 5.1. The curve follows the general pattern for a metal with an initial elastic range followed by hardening. To predict values for Young's modulus only the points in the elastic range were used. The specific data points collected during this interval are marked as crosses in the figure. As can be seen ten sample points exist in the elastic range for this sample. The number of data points in the elastic interval varied between different samples but all samples had between 9-21 data points in the elastic range. This might be a little too low, compared with the required 50 that is needed when doing testing according to standard [9].

Engineering stress-strain curve
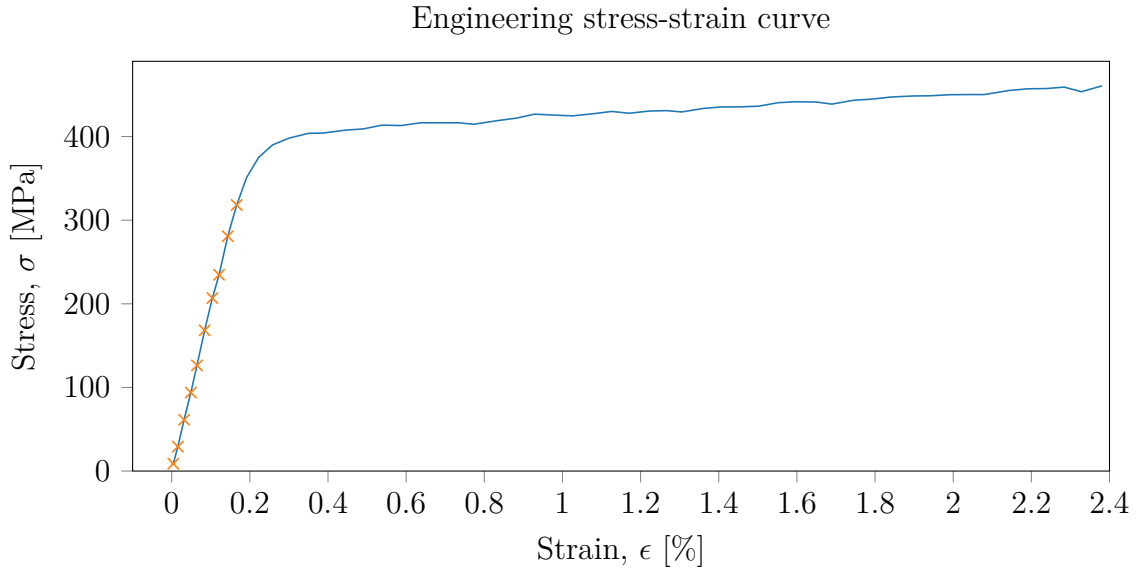
Figure 5.1: Engineering stress as function of engineering strain for test specimen S0_PLATE_A_10_01_A. As can be seen there are roughly ten sample points during the elastic range of the curve.

From the stress-strain curves Young's modulus can be determined by a linear fit to the curve that lies within the elastic interval. For each test specimen it was identified what time frames of the DIC data that could be considered to lie within the elastic range of the stress-strain curve. Depending on which data points that were used within this range, the resulting value of Young's modulus differed somewhat. Four evaluations based on different intervals of data points were therefore made for each sample to investigate the impact of intervals and to illustrate the differences. First interval includes all points that seemingly occur before leaving the elastic range, as depicted in Figure 5.1. The estimations based on the first interval is also denoted E_{DIC} for later use. The second interval is similar to the first but excludes the two endpoints of the first interval. By dividing the second interval into two groups, the third and fourth interval are obtained.

A clarification of which points that were included in interval two to four can be seen in Figure 5.2. A summation of all predictions can be seen in Table 5.1.
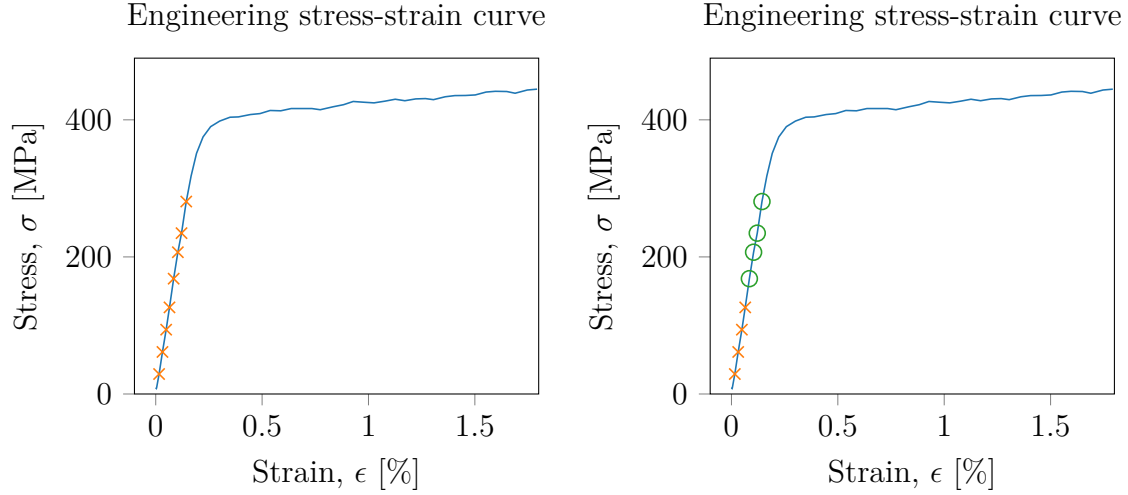

Figure 5.2: Engineering stress as function of engineering strain for test specimen S0_PLATE_A_10_01_A. The left image shows the points included in the second interval. The right image shows the points in interval three as orange crosses and the points in interval four as green circles.

Table 5.1: Young's modulus obtained as the slope of the stress-strain curves obtained from the DIC data listed together with the number of data points in the elastic range. The four intervals are then subsets of the total set of data points.

Test specimen name	Data points	1:st	2:nd	3:rd	4:th
S0_PLATE_A_10_01_A	10	194 GPa	197 GPa	198 GPa	188 GPa
S0_PLATE_A_15_01_A	15	210 GPa	212 GPa	224 GPa	203 GPa
S0_PLATE_A_20_01_A	21	190 GPa	193 GPa	197 GPa	179 GPa
S0_PLATE_A_30_01_A	11	198 GPa	199 GPa	193 GPa	197 GPa
S0_PLATE_A_30_02_A	9	192 GPa	193 GPa	193 GPa	193 GPa
S0_PLATE_A_40_01_A	11	141 GPa	132 GPa	68 GPa	85 GPa
S0_PLATE_T_10_01_A	12	228 GPa	230 GPa	234 GPa	224 GPa
S0_PLATE_T_15_01_A	17	218 GPa	217 GPa	224 GPa	216 GPa
S0_PLATE_T_20_01_A	17	220 GPa	221 GPa	216 GPa	223 GPa
S0_PLATE_T_30_01_A	10	210 GPa	210 GPa	212 GPa	209 GPa
S0_PLATE_T_30_02_A	10	199 GPa	202 GPa	197 GPa	198 GPa
S0_PLATE_T_40_01_A	9	197 GPa	199 GPa	203 GPa	195 GPa

Except from sample S0_PLATE_A_40_01_A, no samples varied more than 20 GPa between lowest estimation and highest estimation and considering the centered intervals, 1 and 2, no samples varied more than 3 GPa. Again except from sample S0_PLATE_A_40_01_A, the values are in reasonable range for steels. To get an idea of why S0_PLATE_A_40_01_A did not provide as good results as the others, the engineering stress-strain curve for that sample is depicted in Figure 5.3. As can be seen here the data from DIC has too much variation. This constitutes a restriction in how good E can be determined for that sample. With only few points and a steep slope, small errors in the data can have a big impact on the results. With more data points collected during the elastic range, the variations due to choice of interval could possibly be reduced further and possible outliers could be distinguished and safely removed from the data and thus improve the results for samples such as S0_PLATE_A_40_01_A.
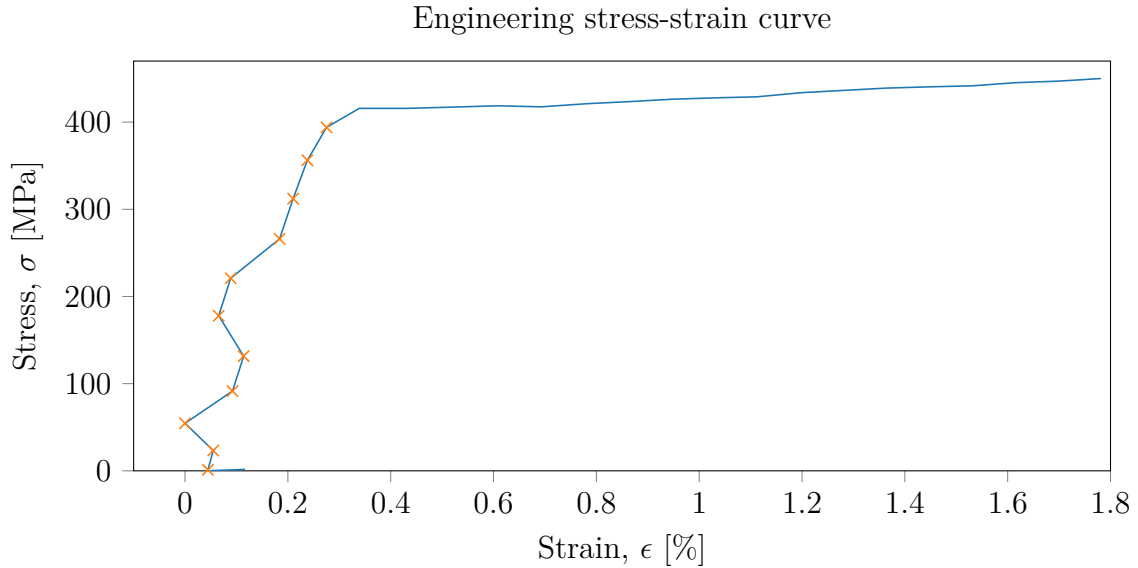

Figure 5.3: Engineering stress as function of engineering strain for test specimen S0_PLATE_A_40_01_A, as can be seen the points in the elastic range are not aligned and thereby restricts the ability to make valid predictions for E.

To get a better overview, the results from Table 5.1 are plotted in Figure 5.4. Young's modulus is plotted as a function of the thickness of the plate from which the specimen was extracted. The rolling direction compared to sample extraction are marked as circles for the samples cut transverse to rolling direction and the crosses for the samples cut along the rolling direction. In this project isotropy was assumed, but the rolling direction could be investigated further as a part of an anisotropic assumption.
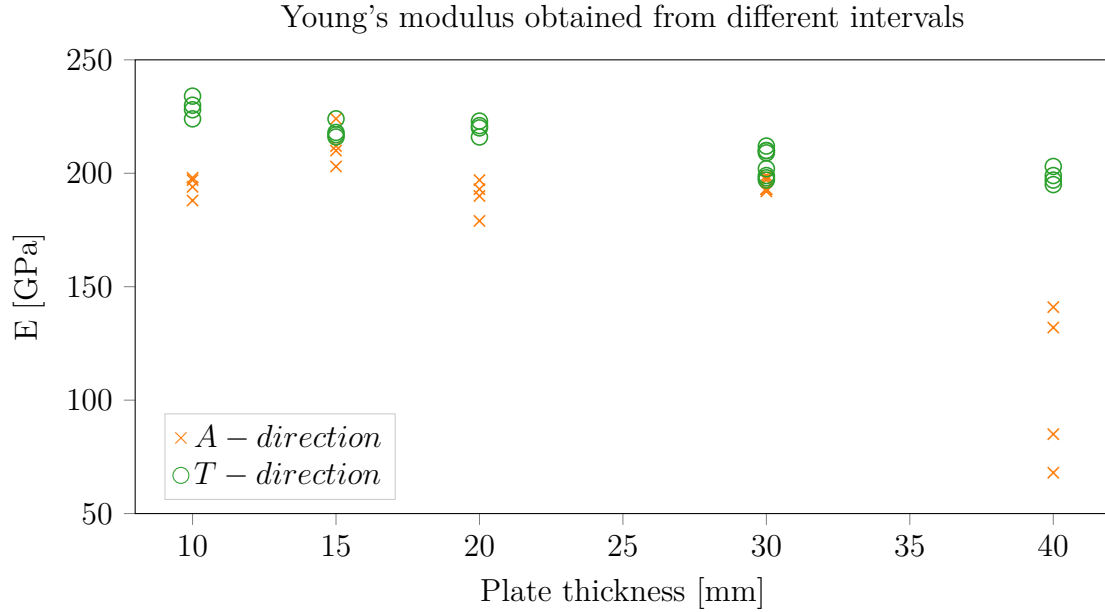
Figure 5.4: The values obtained for Young's modulus sorted by plate thickness and sample direction.

5.1.2 Global estimation and calibration

After analysing the DIC data and obtaining initial guesses for Young's modulus the next step was to try calibrating the FE models based on the DIC data. A global parameter search preceded an optimisation with the Nelder-Mead method.

Since the variation between the first two of the chosen elastic intervals were small, the first interval has been used for the global estimation and calibration. The global estimation served as a check to see if the method provides reasonable results and to observe what initial guess that is suitable for calibration. The values for the three residuals that were defined in equations 4.1-4.3, R_F, $R_{\mathbf{u}_1}$ and $R_{\mathbf{u}_2}$, were evaluated for all combinations of the parameter sets for E and ν.

Figure 5.5 shows how the values for each residual depended on the material parameters for test specimen S0_PLATE_T_30_01_A. For this specific global estimation the parameter space for E was set to $E \in [200, 220]\,GPa$ with $5\,$GPa spacing. The parameter space for ν was set to $\nu \in [0.25, 0.35]$ with 0.05 as spacing. As can be seen in the figure, different residuals depend on different material parameters.
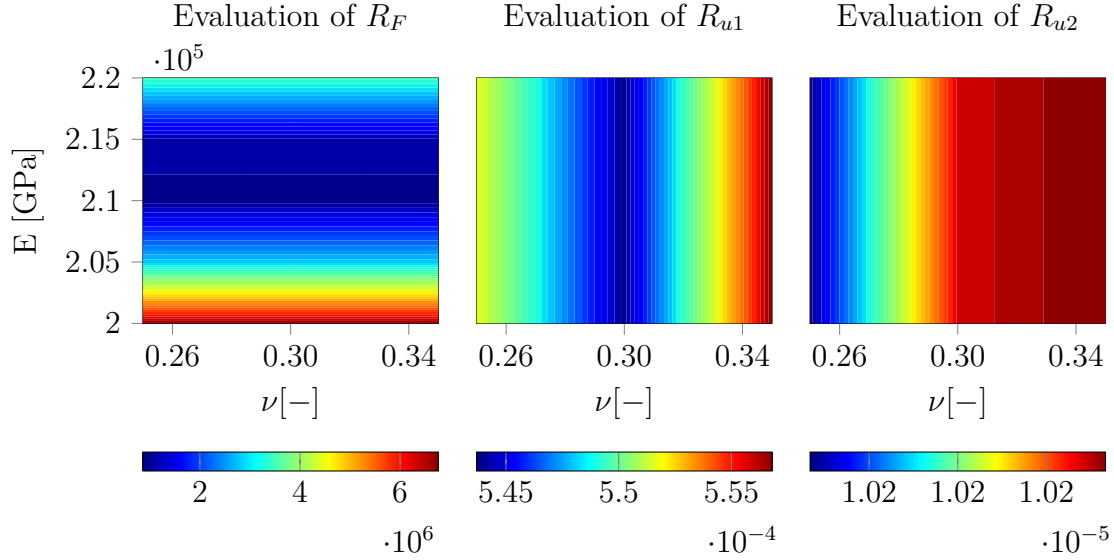

Figure 5.5: The three residual matrices obtained for test specimen S0_PLATE_T_30_01_A. As can be seen the residual R_F only depends on E and the residual $R_{\mathbf{u}_1}$ only depends on ν. The last residual, $R_{\mathbf{u}_2}$, is almost constant over the interval, thus independent of the elastic material parameters.

This was expected for R_F since the material is assumed to be linear and the loading is axial and thus the axial reaction forces depend only on the prescribed elongation and the elastic modulus. It was also expected for $R_{\mathbf{u}_1}$ since ν depends on the prescribed elongation and the thickness in the radial direction. That $R_{\mathbf{u}_2}$ seems to be independent of the material parameters is also reasonable since with the total elongation prescribed and the assumption of elasticity all points will evenly spread independent of the material. Last thing to be noted is that the values provided from R_F are much larger than the ones obtained from $R_{\mathbf{u}_1}$ and $R_{\mathbf{u}_1}$, thus indicating that the weight factors need to be considered when constructing the full objective function that is needed when more material parameters are included.

Based on the direct relationship between the residuals and material parameters, the following analysis only uses R_F for determination of E and $R_{\mathbf{u}_1}$ for determination of ν. The grid was evenly spaced by $5\,$GPa or $10\,$GPa for most cases, and ν was initially set to 0.25, 0.3 and 0.35. The value of E that generates the lowest value in the global investigation is denoted E_{glob} and were used as an initial guess for the Nelder-Mead optimisation routine.

Table 5.2 lists the values of E that were obtained by the three different approaches. E_{DIC} is the value obtained from the initial analysis of the DIC data that was discussed in section 5.1.1, E_{glob} is the optimum choice based on the global search and E_{opt} is the refined value after applying the optimisation routine.

Table 5.2: The values of E that were obtained by the three different approaches.

Test specimen name	E_{DIC}	E_{glob}	E_{opt}
S0_PLATE_A_10_01_A	194 GPa	200 GPa	197.7 GPa
S0_PLATE_A_15_01_A	210 GPa	210 GPa	213.8 GPa
S0_PLATE_A_20_01_A	190 GPa	190 GPa	186.5 GPa
S0_PLATE_A_30_01_A	198 GPa	200 GPa	197.9 GPa
S0_PLATE_A_40_01_A	141 GPa	175 GPa	177.1 GPa
S0_PLATE_T_10_01_A	228 GPa	230 GPa	227.9 GPa
S0_PLATE_T_15_01_A	218 GPa	220 GPa	224.8 GPa
S0_PLATE_T_20_01_A	220 GPa	210 GPa	213.8 GPa
S0_PLATE_T_30_01_A	212 GPa	210 GPa	212.5 GPa
S0_PLATE_T_30_02_A	199 GPa	195 GPa	194.0 GPa
S0_PLATE_T_40_01_A	197 GPa	190 GPa	191.1 GPa

From the initial analysis of the DIC data it was concluded that the data points in the elastic range were too few to accurate determine Young's modulus, thus the results from the three different methods are not expected to be identical. What is encouraging is that E_{opt} and E_{DIC} have similar values and thus indicates a working calibration method. An illustration of how well the forces are predicted can be seen in Figure 5.6 where force is plotted as function of time.
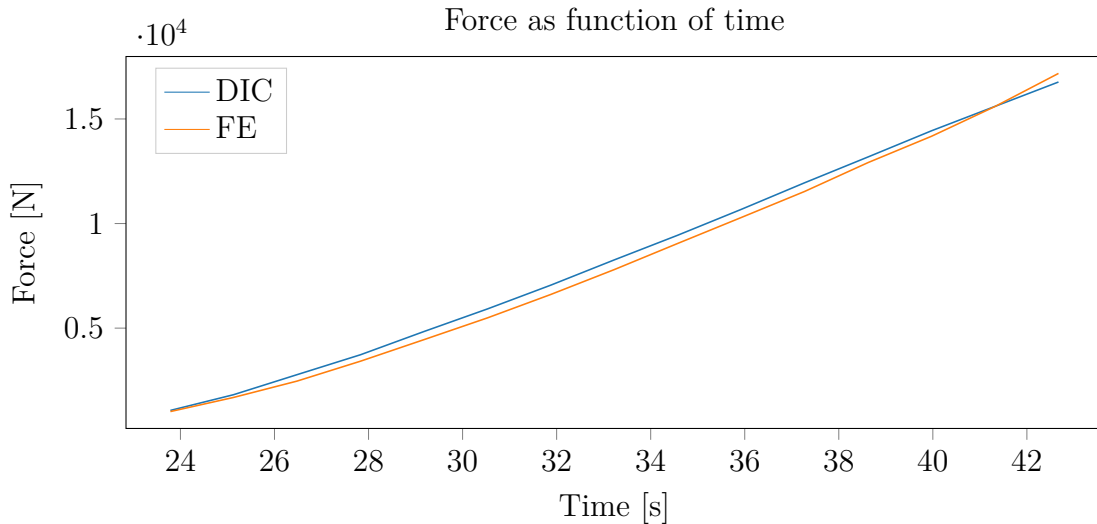

Figure 5.6: The force obtained from experimental data and the force obtained by the simulations as function of time during the elastic range for test sample S0_PLATE_A_15_01_A.

That E_{opt} is close to E_{glob} works as a confirmation of that the Nelder-Mead optimisation routine runs properly, something that will be of more significance when increasing the complexity of the objective function.

When it comes to Poisson's ratio, it was possible to find minimas for some samples but not all of them when performing a global search. For the samples not obtaining 0.3 as mimima, the parameter space were extended to include 0.2 and 0.4 in the parameter space. For samples that did find a minima at 0.3 in the global search, the interval spacing was decreased to be 0.01 instead. A summary of the results for Poisson's ratio is included in Table 5.3. ν_{min} is the minimum value that were tested and ν_{max} was the maximum value that was tested when trying to find a minima of the objective function.

Table 5.3: The range of ν that were used during the global investigation of the samples together with the optimal choice based on the global search. As can be seen only six of the samples succeeded in predicting an acceptable value of 0.29 or 0.3.

Test specimen name	ν_{min}	ν_{max}	ν_{opt}
S0_PLATE_A_10_01_A	0.2	0.4	0.4
S0_PLATE_A_15_01_A	0.25	0.35	0.3
S0_PLATE_A_20_01_A	0.25	0.35	0.3
S0_PLATE_A_30_01_A	0.2	0.35	0.2
S0_PLATE_A_40_01_A	0.2	0.4	0.35
S0_PLATE_T_10_01_A	0.2	0.4	0.4
S0_PLATE_T_15_01_A	0.25	0.35	0.3
S0_PLATE_T_20_01_A	0.25	0.35	0.29
S0_PLATE_T_30_01_A	0.25	0.35	0.29
S0_PLATE_T_30_02_A	0.25	0.35	0.25
S0_PLATE_T_40_01_A	0.25	0.35	0.3

The samples for which the global search resulted in a ν with value 0.2 or 0.4 were considered to be unlikely when compared to normal values for ν for steel. When examining the reason of the unlikely values, it was discovered that the deviations in the radial coordinates over time were so large that the actual displacements became to small to give any reasonable values.

An example of this can be seen in Figure 5.7. This could possibly be avoided by time averaging the radius over time, thereby making the values more robust. More sample points during the elastic range could also improve the results. To get the calibration working for Poisson's ratio, there needs to be better pre-processing of the data.
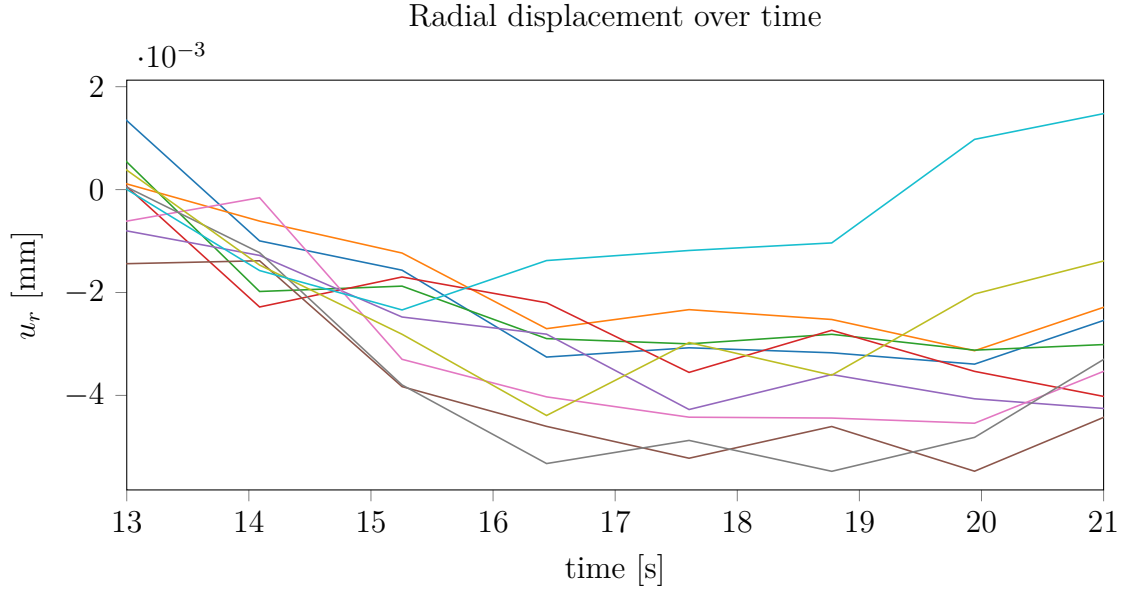

Figure 5.7: The radial displacement during the elastic interval for test sample S0_PLATE_T_10_01_A. The displacement is taken from 10 sample locations over the sample and tracked over time. It can be seen that none of the displacements are strictly decreasing as expected, but instead varying over time. However it should be noted that the displacements are very small, only a few μm.

5.2 Case 2: Estimation of plastic parameters

When expanding the material model to include linear hardening two more parameters were included in the material model. This section will go through the results for the material parameters σ_y and H that were obtained when analysing the DIC data and when using the DIC data to calibrate the FE models.

5.2.1 Initial estimation based on DIC data

The true stress as function of true strain were plotted for the DIC data associated with each individual test specimen.

The true stress-strain curve from sample S0_PLATE_A_10_01_A can be seen in Figure 5.8. This curve corresponds to the engineering stress-strain curve seen in Figure 5.1 earlier.
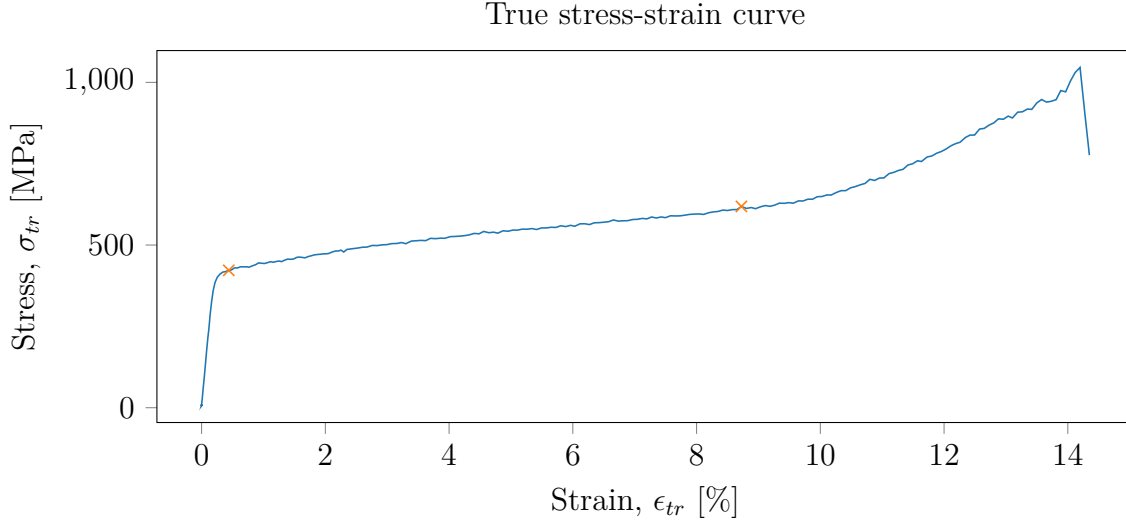

Figure 5.8: True stress-strain curve for test sample S0_PLATE_A_10_01_A. The crosses marks the point of yield stress and the point of ultimate stress obtained from the engineering stress-strain curve.

As described in section 3.1, the predicted offset yield strength, σ_o, was determined according to the offset-yield method and will in this work serve as an initial guess of σ_y. The slope between the point of yield stress and the point of ultimate stress were used to predict the linear hardening constant, H, according to equation 3.3. A summation of all values and predictions can be seen in Table 5.4.

Table 5.4: The values obtained for the true stresses and strains related to the offset-yield method and ultimate tensile strength are listed together with the calculated value of H.

Test specimen name	$\sigma_{o,tr}$	$\sigma_{u,tr}$	$\epsilon_{o,tr}$	$\epsilon_{u,tr}$	H
S0_PLATE_A_10_01_A	422 MPa	619 MPa	0.0044	0.0872	2370
S0_PLATE_A_15_01_A	447 MPa	626 MPa	0.0040	0.1061	1753
S0_PLATE_A_20_01_A	464 MPa	631 MPa	0.0043	0.1175	1470
S0_PLATE_A_30_01_A	444 MPa	581 MPa	0.0046	0.1225	1160
S0_PLATE_A_30_02_A	438 MPa	622 MPa	0.0044	0.1011	1900
S0_PLATE_A_40_01_A	424 MPa	622 MPa	0.0049	0.1127	1681
S0_PLATE_T_10_01_A	473 MPa	634 MPa	0.0043	0.1095	1536
S0_PLATE_T_15_01_A	466 MPa	600 MPa	0.0042	0.1015	1375
S0_PLATE_T_20_01_A	482 MPa	623 MPa	0.0044	0.0860	1727
S0_PLATE_T_30_01_A	435 MPa	584 MPa	0.0037	0.1091	1419
S0_PLATE_T_30_02_A	459 MPa	629 MPa	0.0043	0.0861	2080
S0_PLATE_T_40_01_A	430 MPa	595 MPa	0.0043	0.0834	2082

5.2.2   Global estimation based on force residual

After analysing the DIC data and obtaining initial guesses for the two material parameters associated to the linear elastic material model, the next step was to try calibrating the FE models based on the DIC data. A global search was used to investigate how the residuals would behave and to find global minimas for the parameters.

To make it easier to observe the behaviour of the residuals ν was fixed to 0.3 and E was set to E_{DIC} for each sample. The values for the three residuals, R_F, $R_{\mathbf{u}_1}$ and $R_{\mathbf{u}_1}$, were then evaluated for all combinations of material parameters $\sigma_{o,tr}$ and H. Figure 5.9 shows how the values for each residual depended on the material parameters for test specimen S0_PLATE_A_15_01_A.
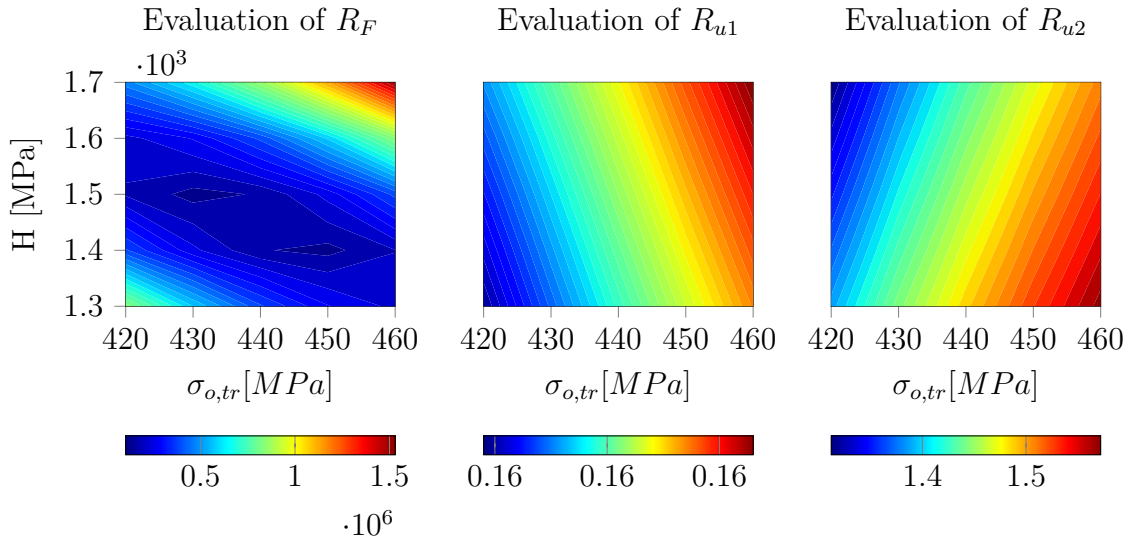

Figure 5.9:   The three residual matrices obtained for for test specimen S0_PLATE_A_15_01_A. As can be seen all residuals show some correlation between $\sigma_{o,tr}$ and H, but the greatest correlation is obtained from R_F

For this specific global estimation the parameter space for $\sigma_{o,tr}$ was set to $\sigma_{o,tr} \in [420, 460]\,GPa$ with $10\,$MPa spacing. The parameter space for H was set to $H \in [1300, 1700]$ with 0.05 as spacing. As can be seen in the figure, these parameters are correlated unlike in the linear elastic case. To run a good calibration the weighting needs to be considered, something that remains to be done. However, R_F seemed to be the dominating term as in the case for Young's modulus. So to get a preview of how well the results could be, the value of R_F was used when performing a global estimation of $\sigma_{o,tr}$ and H.

The results for the specimens are summarised in Table 5.5. A visualisation of how well the simulated results corresponds to the data obtained from DIC can be seen in Figure 5.10. Even though only a linear hardening model was used, the result agrees fairly well between the two values. If implementing more complex material models in the future would be a good possibility to improve these results.

Table 5.5: The values of $\sigma_{o,tr}$ and H obtained from the estimation based on DIC listed and from a global estimation based on the force residual respectively.

| Test specimen name	$\sigma_{o,DIC}$	$\sigma_{o,glob}$	H_{DIC}	H_{glob}
S0_PLATE_A_10_01_A	422 MPa	420 MPa	2370	2000
S0_PLATE_A_15_01_A	447 MPa	430 MPa	1753	1600
S0_PLATE_A_20_01_A	464 MPa	460 MPa	1470	1400
S0_PLATE_A_30_01_A	444 MPa	420 MPa	1160	1200
S0_PLATE_A_30_02_A	438 MPa	440 MPa	1900	1900
S0_PLATE_A_40_01_A	424 MPa	430 MPa	1681	1600
S0_PLATE_T_10_01_A	473 MPa	450 MPa	1536	1300
S0_PLATE_T_15_01_A	466 MPa	440 MPa	1375	1400
S0_PLATE_T_20_01_A	482 MPa	470 MPa	1727	1600
S0_PLATE_T_30_01_A	435 MPa	420 MPa	1419	1400
S0_PLATE_T_40_01_A	430 MPa	440 MPa	2082	2000
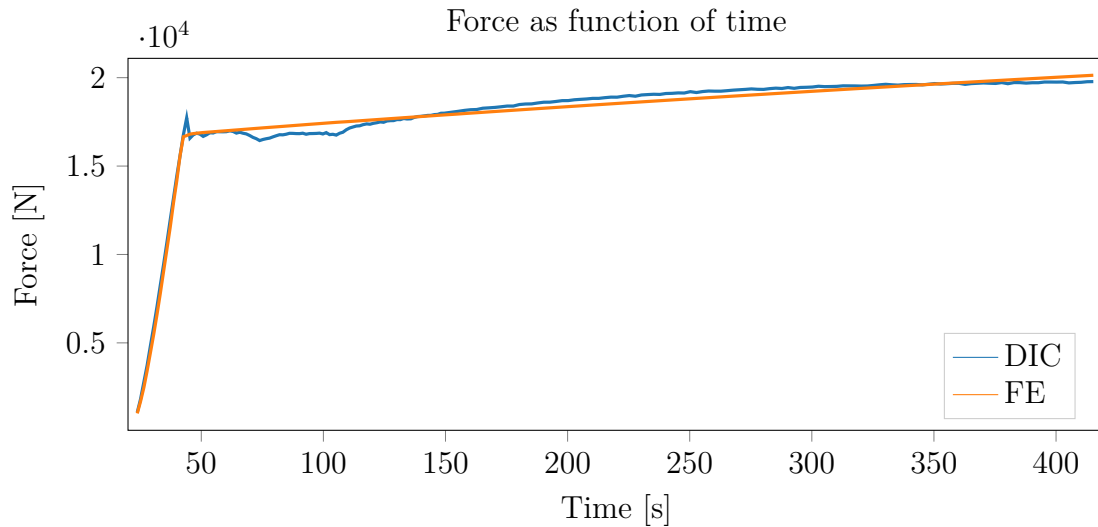
Figure 5.10: The force obtained from experimental data and the force obtained by the simulations as function of time for test sample S0_PLATE_A_15_01_A.

5.3 Case 3: Determination of fracture location

With the help of the calculated cylindrical coordinates and the applied force, the true stress as a function of length could be determined for the test specimens. This information would not be available without the DIC data and was therefore of interest to investigate further. The true stress was therefore plotted as function of length and it was discovered that a stress concentration became visible for the samples very early during the loading. For most cases the early stress concentration coincided with the location where the necking and later fracture of the material occurred.

Since the FE models were constructed from the coordinates obtained from DIC analysis, the actual geometry was reflected instead of the nominal geometry. This resulted in an early indication of where the necking would occur, in accordance with the examination of DIC data only. Figure 5.11 illustrates the stress calculated over the test sample S0_PLATE_A_10_01_A. The true stress is calculated for the DIC data and is seen at the top. The von Mises stress calculated by Abaqus can be seen in the middle and footage of the specimen after fracture can be seen at the bottom. The magnitude of the stress is not included since only the stress concentration is of interest. It appears that the simulations predict failure in the same area as the DIC data shows.
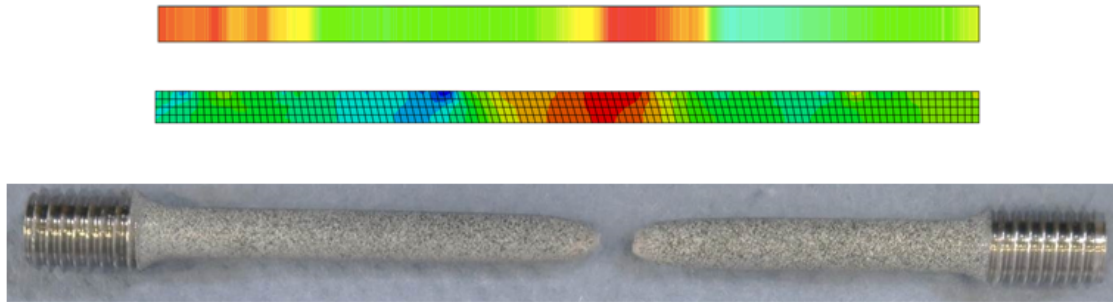

Figure 5.11: All three images are visualisations of test specimen S0_PLATE_A_10_01_A. The top image is the true stress calculated for the surface of the specimen based on the experimental DIC data. The middle image is the von Mises stress calculated in Abaqus after using the radii calculated from DIC data, it shows the stress distribution from the center of the specimen to the surface. The bottom image shows an actual footage of the test sample that was taken after fracture. Both of the two top images are taken from the elastic interval of the test, thus indicating that the area of fracture could be discovered early.

To get a comprehensive comparison of when the necking area can be distinguished the axial coordinate of the highest true stress was tracked over time. This was made to see when the location stabilised around the axial coordinate where necking started to occur.

Figure 5.12 shows a sketch of a specimen where the total length a_{tot}, axial value of where the necking occurs, a_{br}, and the axial value when the location started to stabilise, a_{in}. The location of maximum stress was considered stabilised when the value of a stayed within a certain range from the final breaking spot. This range was chosen to be $\pm 5\%$ of the specimens total length. This condition can be expressed as

$$a_{rel} = \frac{|a - a_{br}|}{a_{tot}} \leq 0.05 \tag{5.1}$$

and a_{in} becomes the first value of a that fulfils this condition before it stays valid for the remaining time. An example of how the maximum true stress changes over time can be seen in Figure 5.13.
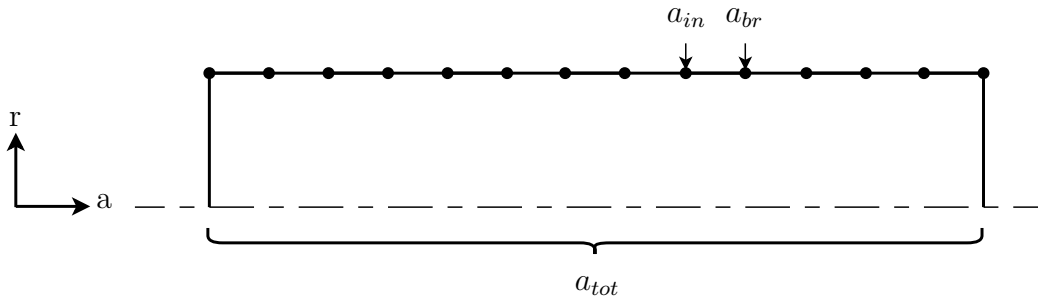

Figure 5.12: Sketch of a test specimen with the notation used when examining the location of fraction. The total length of the specimen measured by DIC is denoted a_{tot}, a_{br} denotes the axial value of the node where the specimen breaks, a_{in} is the axial value when r_{min} starts to stabilise.
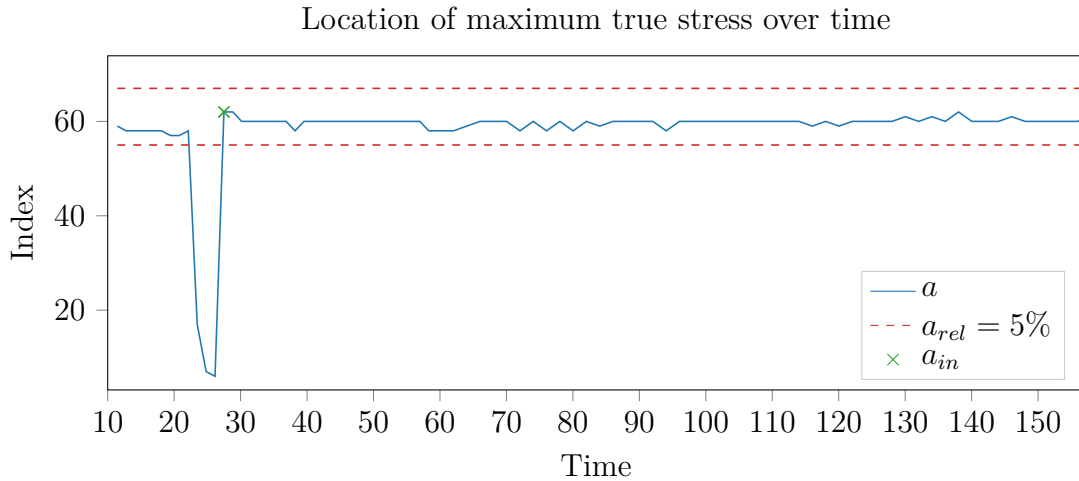

Figure 5.13: The index of the axial coordinate a that has the maximum true stress as a function of time for test specimen S0_PLATE_A_40_01_A. The value is considered stabilised when constantly being located between the two dashed lines. As can be seen the value stabilises early at a_{in} and then only varies with a few indices before maximum stress is reached after 157 s.

46

The time when a_{in} is reached is called time of initiation and is denoted t_{in}. A summary of time of initiation, t_{in}, and relative distance from failure spot, a_{rel}, can be seen in Table 5.6. The times refer to time after load is applied, thus neglecting some data points at the beginning. t_{max} is the time when the maximum stress is reached and the relative time is determined as $t_{rel} = \frac{t_{in}}{t_{max}}$. As can be seen, most cases predicts a spot closer than 5.0 % of the specimens total length at a time long before the maximum stress is reached. Only for a third of the specimens, the initiation of stress concentration is confirmed after reaching the offset-yield stress. For the rest, the stress concentration is found during the elastic interval. A cumulative plot over the stress concentration initiation can be seen in Figure 5.14.

Table 5.6: Time of initiation of stress concentration listed together with the time of maximum stress and the initiation time relative to time of maximum stress. The time when reaching the offset-yield stress is listed as t_o as reference.

| Test specimen name	a_{rel}	t_{in}	t_o	t_{max}	t_{rel}
S0_PLATE_A_10_01_A	2.6%	0 s	19 s	230 s	0
S0_PLATE_A_15_01_A	1.8%	72 s	27 s	393 s	0.183
S0_PLATE_A_20_01_A	2.8%	0 s	33 s	382 s	0
S0_PLATE_A_30_01_A	3.2%	52 s	17 s	209 s	0.249
S0_PLATE_A_30_02_A	4.0%	0 s	17 s	173 s	0
S0_PLATE_A_40_01_A	3.1%	19 s	19 s	195 s	0.097
S0_PLATE_T_10_01_A	4.3%	80 s	19 s	287 s	0.279
S0_PLATE_T_15_01_A	2.4%	34 s	28 s	376 s	0.090
S0_PLATE_T_20_01_A	2.2%	0 s	32 s	279 s	0
S0_PLATE_T_30_01_A	2.4%	3 s	15 s	185 s	0.016
S0_PLATE_T_30_02_A	3.2%	17 s	17 s	148 s	0.115
S0_PLATE_T_40_01_A	3.1%	14 s	15 s	143 s	0.098
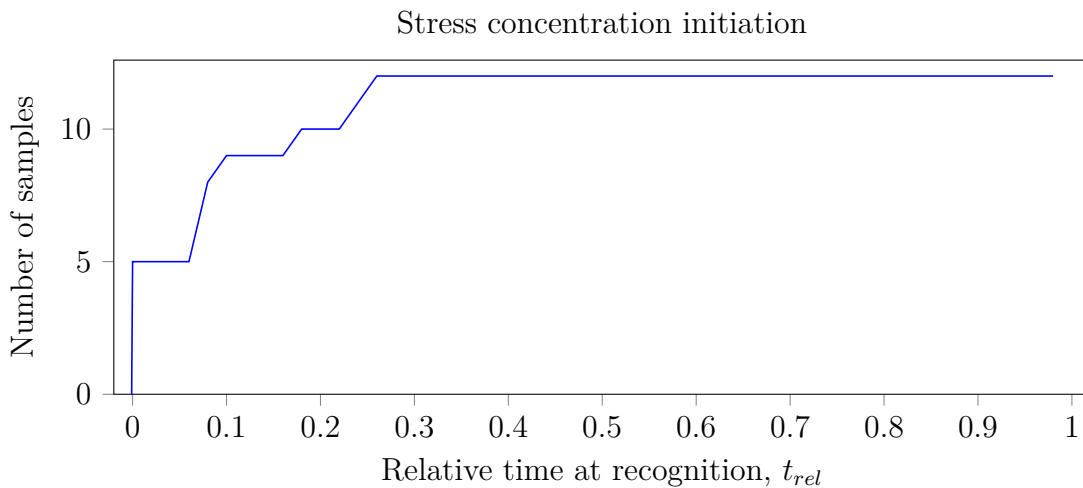
Figure 5.14: A cumulative plot showing when the necking point is distinguished compared to time of maximum stress for the 12 samples.

For most samples the location of the necking can be determined very early compared to failure. This result indicates that after only obtaining the geometry, the area of where the necking will occur can be made visible by the simulations. For test specimen S0_PLATE_T_10_01_A, longer time than for other samples were needed to define this area. While inspecting the contour of the surface, seen in Figure 5.15, this can be tracked to having a small radius close to the end of the specimen. The final breaking point was at the axial value $a = 29.4\,\text{mm}$.
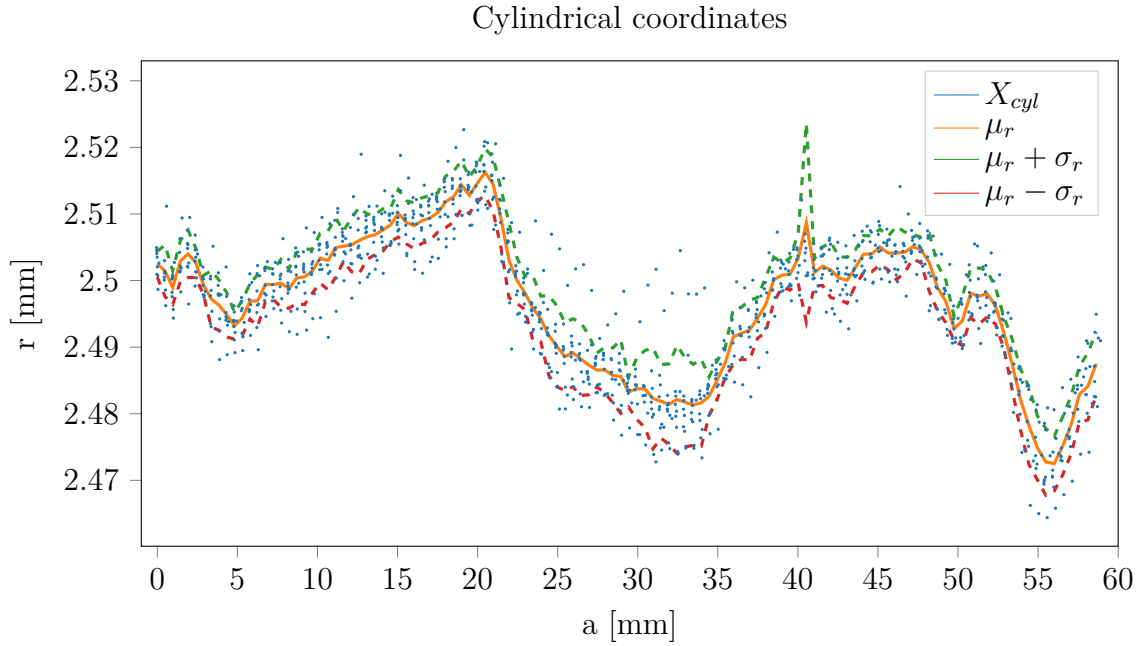

Figure 5.15: The surface contour for test specimen S0_PLATE_T_10_01_A after 15 s. The small radius at the end of the sample prevents the script from recognising the middle as the weakest part as early as for other samples.

5.4 Averaging data for improvement

What has not fully been investigated is how small abnormalities in the data affects the results. As found when trying to calibrate for Poisson's ratio, the radial displacements are small and deviations over time are not constantly decreasing as would have been expected when increasing the tensile force. The conclusion from that is that the deviations in the data are in the same order as the actual displacements. Small variations in the data from different DIC frames give miscalculations of displacements. What might be of interest is to investigate further the influence of facet size chosen in Aramis, as mentioned earlier larger facets provide data with less deviations but decreases the solution. Another possible action to make the values more robust for small deviations in time would be to consider time deviations when fitting the cylindrical coordinate system to the data.
All displacements measured by DIC is based on the difference in position between

the first frame and the actual frame, this could lead to errors if the first data frame holds large deviations compared to the rest. This could probably be helped by averaging the initial coordinates based on multiple frames as well. If making more experiments, more frames could be collected before applying the force, thus leaving a couple of frames from which an average could be calculated and used as initial values.

Averaging could also be of interest in the early frames when considering the displacement that is sent into the FE model. As of the current model the boundary condition is based on the displacement at the highest axial value, during the elastic range the displacements are not so large so small deviations between frames would get larger impact.

6
Concluding remarks

With the aim to obtain a general method that uses DIC to calibrate an FE model some interesting things have been found but there are still much to investigate in the future. This chapter will summarise important notes regarding the work and also point out what have been learnt during the project together with ideas for future work.

6.1   Summary and important results

During the project, a method that uses DIC data to setup an FE model and find the material parameters that minimises the deviation between this model and experimental data for a specific material model has been obtained. Pre-processing of the DIC data was performed to obtain a local cylindrical coordinate system that would simplify the comparison with simulations of tensile tests. During this phase the assumption of axisymmery and a varying radius were introduced. The second phase of the project consisted in creating FE models with the help of Abaqus script and to connect the data from experiments and simulations with a Python script. Three different cases studies were then performed to estimate material parameters based on the DIC data and by using the calibration method.

Even though steel is not the material that could get the most benefit from a more detailed calibration method, it has served as a great help to understand features of the DIC and important principles of the method.

It was a positive result that the DIC data obtained from Aramis were accurate enough to obtain cylindrical coordinates with a small standard deviation. The discovery that the radius varied over the sample was of importance to early predict the area where the necking would occur only based on the DIC data. When using the actual geometry for setting up the FE models, those models also predict the area of necking good. This highlights that accurate description of the geometry can have a crucial impact when constructing a model even for such a simple geometry. The small deviation between necking point seen from the DIC data, FE simulation data and the images taken of the specimens shows that the calculation of cylindrical coordinates are at least sufficiently good and brings information to the sample.

The method of the calibration works but to get reliable results, data of good quality needs to be used in the calibration routine. Since the available data was not collected specifically for this project no thought was put into the need of having much data in the in the elastic range of the stress-strain curve. The lack of this type of data became a limiting factor when trying to determine Young's modulus.

This project has provided a good start to the evaluation of the effects of calibrating FE models with the use of DIC. With a working method of comparing experimental data obtained with DIC to simulated data from an FE software, there should not be to much of an effort to invoke more complex models and expand the model to get more results.

6.2 Suggestions for future work

Much time was spent on the investigation of the DIC data and to get the method working, therefore there are several things that are interesting to examine in the future.

As mentioned above, a greater amount of data collection over the elastic range would be of interest to get a better measure of how well the calibration in itself works. This work indicates that the calibration works fairly well even for small amount of data but is not fully reliable. More sample points in the elastic range would also constitute a better foundation foundation to investigate Poisson's ratio. An additional data collection would thus be needed for this purpose.

It is also of interest to invoke more material models to get an overall comparison of how well the calibration works. This is something that could be useful when considering other materials with a more complex structure. Additional data would be of interest for this as well, to obtain more complex data than for steel. When considering more material models the error function needs to be further developed. When only a few parameters are studied the error from the different terms could be used separately to calibrate different parameters, when more complex models are used the weighting of the different terms become important and needs to be taken into account.

The current focus have been on the calibration of the material models, to verify the calibration some organised validation of the results needs to be done as well.

Bibliography

[1]   Hubert W. Schreier Michael A. Sutton Jean-José Orteu. *Image Correlation for Shape, Motion and Deformation Measurements: Basic concepts, Theory and Applications*. Vol. 1st edition. Springer, 2009.

[2]   E. Dartfeldt. "Series 0 - Test plan and results". Confidential. 2017.

[3]   Klaus-Jürgen Bathe. *Finite Element Procedures*. Prentice Hall, 1996.

[4]   Bryan J. Mac Donald. *Practical Stress Analysis with Finite Element*. Glasnevin Publishing, 2011.

[5]   Håkan Johansson Magnus Ekh. "Introduction to parameter identification for constitutive equations". Unpublished.

[6]   Javad Hashemi William F. Smith. *Foundations of materials science and engineering*. Fourth edition. Prentice Hall, 2006.

[7]   SIS - Standardiseringskommissionen i Sverige. *SS 11 21 13: Metalliska material - dragprovstavar för gängbackar - Rundprovstavar typ C*. SIS, 1986.

[8]   Norman E. Dowling. *Mechanical Behaviour of Materials*. Fourth edition. Pearson, 2013.

[9]   European commitee for standardization (CEN). *SS-EN 10225:2009 - Weldable structural steels for fixed offshore structures - Technical delivery conditions*. Brussels: CEN, 2009.

[10]   J. T. B. Overvelde. *Learn Abaqus script in one hour*. 2010. URL: `http://bertoldi.seas.harvard.edu/files/bertoldi/files/learnabaqusscriptinonehour.pdf` (visited on 05/24/2018).

[11]   *Getting Started with Abaqus: Interactive edition*. Simulia. 2014.

[12]   The Scipy community. *scipy.optimize.fmin*. URL: `https://docs.scipy.org/doc/scipy-0.19.0/reference/generated/scipy.optimize.fmin.html` (visited on 05/29/2018).

[13]   *Abaqus Analysis User's Guide*. Simulia. 2014.

Bibliography

A
Abaqus script

Abaqus scripting is an application programming interface connecting to the models and data used by Abaqus. Abaqus scripting is based on the object-oriented Python programming language. All actions that can be made in Abaqus/CAE graphical user interface (GUI) have an equivalent Python statement or block of statements and the actions can thus be performed by Abaqus scripts instead[13]. The scripting is powerful and lets the user combine the functionality of Abaqus and the programming language Python. For tasks that are repetitive, scripting is valuable since it lets the program do all the work. The script can be run inside Abaqus in the GUI but can also be controlled and run from an outer program through the terminal, of which the latter is used mostly during this work. Two scripts are written for the analysis of the tensile tests. The first script uses Abaqus to construct an FE model based on the data from the DIC analysis and call the next script. The second script extracts the desired output from the ouput database that was generated by the first script and writes the results to reports. The content of the scripts are explained more detailed below.

A.1   Script for model setup

To produce FE models corresponding to different tensile tests with varying geometry and material parameters, a script that constructs those models was created. The script is altered to correspond to different setup choices and are designed according to the following work flow:

1. *Parameter definition.* The beginning of the script encloses variables that controls the geometry, material parameters, mesh details, time steps and end displacement for each step.
2. *Creation of part.* The simple geometry of a tensile test specimen is created by a profile sketch that is axisymmetric according to the axisymmetric assumption. The outer edge of the sketch is based on the coordinates obtained from the DIC data analysis.
3. *Material definition.* The material model is chosen together with the current material parameters and assigned to the part.
4. *Creation of instance.*
5. *Creation of sets.* The sets are created to make postprocessing easier, only the values at the surface has corresponding values in the DIC data.
6. *Creation of steps and boundary conditions.* The steps and displacement of the upper end are determined based on the DIC data analysis.

7. *Seeding and meshing of the model.* Seeds the edges of the model to control the mesh structure.
8. *Setup of job.*
9. *Execution of postprocessing script.*

A.2   Script for postprocessing

To automatically handle the output of interest a postprocessing script is constructed. This script reads the results from the output database file that Abaqus produces when running the job on the model database and prints report files. The report files holds information about the axial and radial displacements for the nodes corresponding to the nodes given by DIC and also the reaction forces that are obtained from the nodes at the upper end of the specimen. Step times are also included to verify that the correct files are used. Time steps in Abaqus are there to split up the analysis into sequences, in this work it is primary made to define multiple prescribed displacements of the end.